Since January 2020 Elsevier has created a COVID-19 resource centre with free information in English and Mandarin on the novel coronavirus COVID-19. The COVID-19 resource centre is hosted on Elsevier Connect, the company's public news and information website.

Journal of Cleaner Production 319 (2021) 128599

Contents lists available at ScienceDirect

Journal of Cleaner Production

journal homepage: www.elsevier.com/locate/jclepro

Google Earth Engine based spatio-temporal analysis of air pollutants before and during the first wave COVID-19 outbreak over Turkey via remote sensing

Fatemeh Ghasempour [a], Aliihsan Sekertekin [b,*], Senol Hakan Kutoglu [a]

[a] Department of Geomatics Engineering, Bulent Ecevit University, Zonguldak, 67100, Turkey
[b] Department of Geomatics Engineering, Cukurova University, 01950, Ceyhan, Adana, Turkey

ARTICLE INFO

Handling editor: Bin Chen

Keywords:
Remote sensing
Google earth engine
Air pollution
COVID-19
TROPOMI
Turkey

ABSTRACT

Air pollution is one of the vital problems for the sustainability of cities and public health. The lockdown caused by the COVID-19 outbreak has become a natural laboratory, enabling to investigate the impact of human/industrial activities on the air pollution. In this study, we investigated the spatio-temporal density of TROPOMI-based nitrogen dioxide (NO_2) and sulfur dioxide (SO_2) products, and MODIS-derived Aerosol Optical Depth (AOD) from January 2019 to September 2020 (also covering the first wave of the COVID-19) over Turkey using Google Earth Engine (GEE). The results showed a significant decrease in NO_2 and AOD, while SO_2 unchanged and had slightly higher concentrations in some regions during the lockdown compared to 2019. The relationship between air pollutants and meteorological parameters during the lockdown showed that air temperature and pressure were highly correlated with air pollutants, unlike precipitation and wind speed. Moreover, Purchasing Managers' Index (PMI) data, indicator of economic/industrial activities, also provided poor correlation with air pollutants. TROPOMI-based NO_2 and SO_2 were compared with station-based pollutants for three sites (suburban, urban, and urban-traffic classes) in Istanbul, revealing 0.83, 0.70 and 0.65 correlation coefficients for NO_2, respectively, while SO_2 showed no significant correlation. Besides, AOD data were validated using two AERONET sites providing 0.86 and 0.82 correlation coefficients. Overall, the satellite-based data provided significant outcomes for the spatio-temporal evaluation of air quality, especially during the first wave of the COVID-19 lockdown.

1. Introduction

Air pollution is one of the most important and vital challenges in developing countries, which occurs as a result of rapid urban development, the expansion of the manufacturing industry and the use of fossil fuels in factory, and residential activities (He et al., 2017; Xu and Lin, 2017; Perera, 2017). In recent decades, the issue of pollution and environmental degradation have been among the main concerns at the domestic, regional and international levels (Eckhoff, 2009). Air pollution occurs when large volumes of harmful particles or substances such as gases, particulate matters, and biological molecules enter the Earth's atmosphere. It can also increase the effect of global warming or disease in humans such as Asthma, Bronchitis, shortness of breath, heart attacks and various respiratory allergies (Arya, 1999; Eckhoff, 2009). Among the air pollutant gases, the most critical pollutants in the world's metropolitan areas are carbon monoxide (CO), ozone (O_3), sulfur dioxide (SO_2), nitrogen dioxide (NO_2), Particulate Matters ($PM_{2.5}$ and PM_{10}) (Zhang et al., 2020a). These pollutants are generally emitted from both stationary and mobile resources. Stationary resources involve domestic, residential and industrial activities, while transportation and vehicles that pollute the air by generating pollutants from exhaust fumes and particulate matter are among the mobile sources of the air pollution. In fact, except for SO_2, which is mainly emitted from residential and industrial sources, the other pollutants are generally emitted much more by the vehicles.

Satellite-based remote sensing technology offers an effective solution for long-term spatio-temporal monitoring of air quality under various scales. The use of satellite imagery to monitor air pollution dates back to the 1970s with the utilization of the Advanced Very High Resolution Radiometer (AVHRR), Landsat, and the Geostationary Operational

* Corresponding author.
E-mail address: asekertekin@cu.edu.tr (A. Sekertekin).

https://doi.org/10.1016/j.jclepro.2021.128599
Received 19 January 2021; Received in revised form 6 August 2021; Accepted 8 August 2021
Available online 14 August 2021

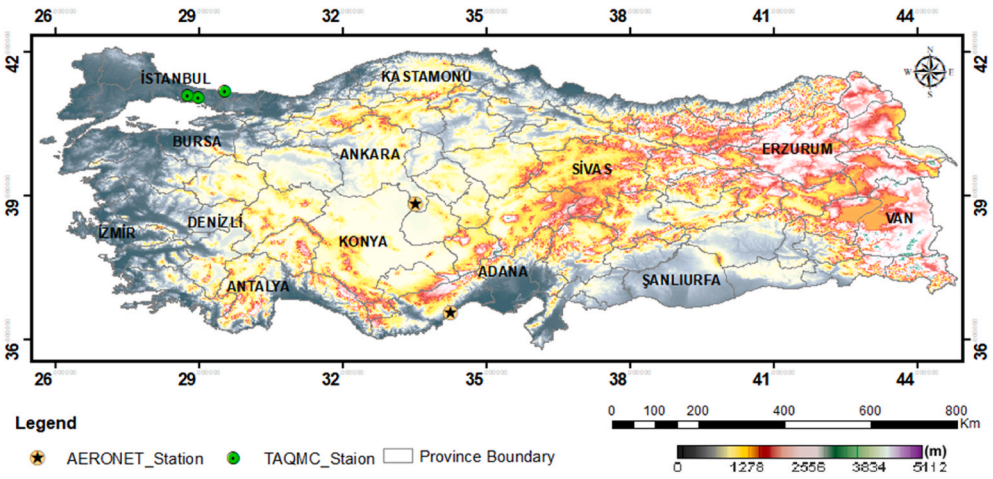

Fig. 1. Illustration of the study area, Turkey, and ground stations via SRTM-DEM.

Environmental Satellite (GOES). In addition, Nimbus-7, European Remote-sensing Satellite-2(ERS-2), Terra, ENVironmental SATellite (ENVISAT), Aqua, Aura, Meteorological OPerational satellite (MetOP), and Sentinel-5 precursor (Sentinel-5P) are among the other satellites that have been frequently used for air quality monitoring since 1978. Concerning the literature, many researchers have studied monitoring, analyzing and retrieval of air pollutants such as Aerosols, NO_2, SO_2, PM_X, CH_4, CO, and O_3 using these remote sensing satellites (Aldabash et al., 2020; Kaplan and Yigit Avdan, 2020; Laat et al., 2020; Lin et al., 2019; Ruoying et al., 2019; Salmabadi and Saeedi, 2019; Wang et al., 2019; Feng et al., 2019; Hajiloo et al., 2019; Wu et al., 2019; Borsdorff et al., 2019; O'Brien et al., 2016; Tzortziou et al., 2018; Xu et al., 2018). The TROPOspheric Monitoring Instrument (TROPOMI) onboard Sentinel-5P, launched on October 13, 2017, is the first Copernicus mission and the latest satellite-based sensor for air quality monitoring (Butz et al., 2012). It has been providing high spatio-temporal resolution data for monitoring the air quality parameters, namely, Absorbing Aerosol Index (AAI or UVAI), O_3, CO, NO_2, SO_2, CH_4, cloud characteristics and formaldehyde (HCHO) (El Khoury et al., 2019).

In addition to the aforementioned satellite-based air pollution studies, in late 2019, monitoring and investigating the effect of coronavirus (COVID-19) lockdown on air pollution has attracted the attention of the scientists as a milestone for air quality management all around the world. Ogen (2020) investigated the relationship between the COVID-19 mortality and long-term exposure to NO_2 pollution via Sentinel-5P in Italy, Spain, France and Germany. The results indicated that the long-term exposure to NO_2 may be one of the most important contributors to fatality caused by the COVID-19 in these regions (Ogen, 2020). Another study was about monitoring the effect of NO_2 concentration on the atmosphere during the lockdown in Spain (Mesas-Carrascosa et al., 2020). They concluded that there was a significant correlation between the level of the population's activity and the reduction in NO_2 values. Metya et al. (2020) used ARIS-derived CO, and NO_2, and OMI-derived SO_2 in India and China during January–April 2020. Their results indicated that the tropospheric NO_2 levels reduced on an average by 17% over India and 25% over China. Besides, approximately 17% reduction was observed in the boundary layer SO_2 especially over the Eastern sector of India, and the 6.5% reduction of CO was determined over north-central China. Nichol et al. (2020) investigated regional air quality indicators over the Beijing–Tianjin–Hebei (BTH) region and other parts of China during the winter of 2019–2020, when the COVID-19 outbreak in China caused reduction in transport and economic activity from November 2019 to February 2020. They stated that, in March and April 2020, Ozone Monitoring Instrument (OMI) satellite-derived NO_2 significantly decreased across China. They also highlighted that the increase in PM2.5 unlike the decrease in NO_2 in BTH and across China is likely due to enhanced production of secondary particulates. Ghahremanloo et al. (2020) utilized SO_2, CO, NO_2 and HCHO from Sentinel-5P, and daily AOD from the Himawari-8 satellite over BTH, Wuhan, Seoul, and Tokyo during February 2019 and 2020. The comparison analysis between 2019 and 2020 indicated the vast pollution reduction in Wuhan with a decline of about 83%, 11%, 71%, 4% and 62% in NO_2, HCHO, SO_2, CO, and AOD, respectively. The finding of Kanniah et al. (2020) determined a notable decrease in tropospheric NO_2 during the lockdown period over the Southeast Asia region. Furthermore, some studies also stated that TROPOMI-based NO_2 observations were decreased during the lockdown period in some of the big European cities, highly populated Chinese cities and North of Italy, respectively (Cersosimo et al., 2020; Fan et al., 2020; Ghasempour et al., 2021; Vîrghileanu et al., 2020). Apart from the satellite-based air pollutant analyses, some researchers also proved the reduction in station-based air pollutants due to the COVID-19 pandemic control strategies (Chen et al., 2021; Nakada and Urban, 2020; Othman and Latif, 2021).

The main objective of this study is to monitor and investigate the spatio-temporal patterns of Sentinel-5P derived air pollutants, namely, NO_2 and SO_2, and MODIS-derived AOD before and during the first wave of the COVID-19 covering the period from January 2019 to September 2020 over Turkey. The COVID-19 lockdown period in Turkey mainly covers the period from March 10 to May 31, 2020 for the first wave, and partly June since the restrictions were gradually loosened in June. Thus, we assumed the lockdown period as of March, April and May in 2020. Although there was a partial lockdown instead of a full lockdown in Turkey for the first wave, it was observed that human activities greatly reduced in this period due to the warnings to control the spread of the virus. As it is clear from the given literature, many studies have been published about the effect of the COVID-19 outbreak on air quality. These studies can be categorized into four distinctive groups including (i) station-based studies, (ii) remote sensing based studies, (iii) combination of the station-based and the remote sensing based studies, and (iv) remote sensing based studies with meteorological/climatological parameters (Karuppasamy et al., 2020; Broomandi et al., 2020; Elshorbany et al., 2021; Mesas-Carrascosa et al., 2020; Metya et al., 2020; Ghahremanloo et al., 2020; Nakada and Urban, 2020; Rojas et al., 2021; Vîrghileanu et al., 2020; Zhang et al., 2020c). Concerning the originality of this research, this study includes a combined analysis of all four approaches mentioned above with also an addition of Purchasing Managers' Index (PMI), which is an indicator of economic/industrial activities. Furthermore, satellite-based pollutants and meteorological parameters were visualized, analyzed and extracted using Google Earth Engine (GEE) open-source geospatial analysis platform, which enables working on JavaScript programming language.

Table 1
List of all datasets used in this study.

Category	Variables	Units	Temporal Resolution	Data Source
Satellite image data of Sentinel-5P	tropospheric_NO2_column_number_density	molec/cm^2	daily	https://developers.google.com/earth-engine/datasets/
	SO2_column_number_density	molec/cm^2		
Satellite image data of MODIS	Optical_Depth_047	*	daily	https://developers.google.com/earth-engine/datasets/
Pollutant Concentration (Turkey Air Quality Monitoring Center)	NO_2, SO_2	μgr/cm^3	hourly	https://www.havaizleme.gov.tr/
ERA5	v_component_of_wind_10m	m/s	monthly	https://developers.google.com/earth-engine/datasets/
	u_component_of_wind_10m	m/s		
	mean_2m_air_temperature	k		
	total_precipitation	m		
	surface_pressure	pa		
AERONET	AOD_500 nm	*	hourly	https://aeronet.gsfc.nasa.gov/
	AOD_440 nm			
PMI	PMI data	*	monthly	https://www.investing.com/economic-calendar/turkish-manufacturing-pmi-1305

2. Study area

Turkey, with 81 provinces and a population of 83.15 million (https://www.nufusu.com/), is a unique country that is lying partly in Asia and partly in Europe at geographical coordinates of 36°–42° N and 26°-45°E. The territory of Turkey has a length of 1660 km from east to west and an area of 780043.00 square kilometers. The average altitude of the country is about 1132 m from mean sea level and there are four different types of climate containing Mediterranean climate, Black Sea Climate, Marmara climate and Continental climate. Ankara, the capital of Turkey, and Istanbul, the country's economic, cultural and historical center are the most populous cities in Turkey. Fig. 1 represents the study area and the ground stations via Digital Elevation Model (DEM) obtained from Shuttle Radar Topography Mission (SRTM).

3. Materials and methodology

3.1. Data collection and preprocessing

In addition to several studies about air pollution monitoring during the COVID-19 pandemic lockdowns (Ghahremanloo et al., 2020; Kanniah et al., 2020; Mesas-Carrascosa et al., 2020; Metya et al., 2020; Nichol et al., 2020; Ogen, 2020; Tobías et al., 2020), we have investigated the impact of the COVID-19 lockdown on the air quality at a national level (over the whole Turkey) for the period from January 2019 to September 2020. As shown in Table 1, we utilized six types of data sets in this study: (a) Hourly NO_2 and SO_2 concentrations from the Turkey Air Quality Monitoring Center (TAQMC), (b) Daily satellite image data of Sentinel-5P NO_2 and SO_2 products from the GEE, (c) Daily satellite image data of MODIS AOD product from the GEE platform, (d) ERA5 Reanalysis climatic and meteorological data, (e) AErosol RObotic NETwork (AERONET) data, and (f) Purchasing Managers' Index (PMI). The connections between the data sets and their usages are presented in the following sections.

3.1.1. Satellite remote sensing data

In this study, we have employed satellite image collections to analyze the spatio-temporal distribution of air pollutants, namely, NO_2, SO_2, and AOD before and during the COVID-19 pandemic lockdown. The daily TROPOMI and MODIS data were used to produce the maps of monthly spatial patterns of the air pollutants. We acquired the tropospheric vertical column density of offline level 3 NO_2 (COPERNICUS/S5P/OFFL/L3_NO2) and the vertical column density at the ground level of offline level 3 SO_2 (COPERNICUS/S5P/OFFL/L3_SO2) from the TROPOMI instrument on board the Sentinel-5P satellite. The TROPOMI is an advanced multispectral imaging spectrometer with nadir-viewing and wavelengths of Ultraviolet–Visible (UV-VIS, 270 nm–495 nm), Near Infrared (NIR, 675 nm–775 nm), and Shortwave Infrared (SWIR, 2305 nm–2385nm). Besides, it is tracking the unique effects of atmospheric gases in different parts of the electromagnetic spectrum. It uses passive remote sensing techniques to reach the target above the atmosphere by measuring the solar radiation reflected by the Earth. The sensor works in a cross direction, with ~2600 km swath width on the ground surface. The nadir view for all spectral bands is 7 × 3.5 km^2, except SWIR bands with 7 × 7 km^2 and UV band with 7 × 28 km^2 (Veefkind et al., 2012). However, in this study, all these Sentinel-5P derived products are delivered in 0.01 arc degree (~1.11 km) spatial resolution from the GEE. In addition to Sentinel-5P data, we collected the daily AOD images of the MODIS (MODIS/006/MCD19A2_GRANULES) onboard the Terra and Aqua satellites with 1 km spatial resolution. Google Earth Engine, with a powerful open-source processing system in JavaScript programming language, enables users to perform calculations, analyze and visualize large volumes of data without the need for powerful systems. The system supports a variety of widely used satellite data such as Landsat, Sentinel and MODIS that are available free of charge.

3.1.2. Turkey Air Quality Monitoring Center (TAQMC) data

Hourly pollutants' concentration data can be gathered from the Turkish air quality real-time release platform (https://www.havaizleme.gov.tr/) administered by the Turkey Air Quality Monitoring Center (TAQMC), one of the major institutions under the Environment and Urban Ministry. The extensive monitoring stations provide continuous hourly pollutant measurements. In this study, we used the ground-based measurements of NO_2 and SO_2 concentrations that were obtained from three hotspots monitoring stations as urban traffic (Beşiktaş), urban background (Başakşehir), and suburban (Şile) stations over the most populous cities in İstanbul. Ground-based NO_2 and SO_2 values were analyzed together with Sentinel-5P derived NO_2 and SO_2 data over the related test sites. A time interval of ±0.5 h was used to match the datasets of TAQMC observations with the satellite pass time. Thus, the hourly pollutant concentrations from the TAQMC were used for the comparison of the data of the ground stations and the satellite acquisitions.

3.1.3. Aerosol robotic network (AERONET) data

The Aerosol Robotic NETwork (AERONET) is a globally ground-based remote sensing aerosol network established and distributed by NASA and PHOTONS. For more than 25 years, the AERONET has been using Cimel Electronique Sun/Sky radiometers to prepare extremely accurate ground truth measurements. In this study, we have used the version 3 level 2 AOD data that have high-quality ground-based assurance for the validation of MODIS AOD products. The AERONET dataset

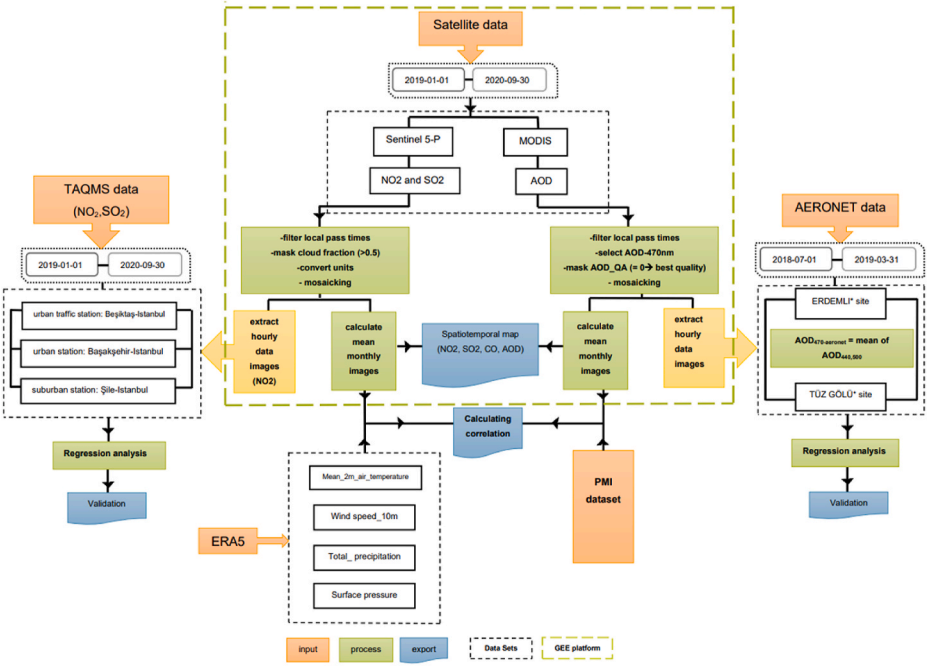

Fig. 2. The workflow illustrating the operations and relations between the methods for the evaluation of air pollutants and related variables.

is divided into 3 quality levels including raw data from level 1, cloud-screened data from level 1.5, and quality assurance data from level 2 (Smirnov et al., 2000). The AERONET version 3 level 2 data may be downloaded from the AERONET website (https://aeronet.gsfc.nasa.gov/The AOD in the AERONET version 2 was semi-automatically controlled in near real-time quality using a cloud-screening method, while the AERONET Version 3 algorithm provides fully automated cloud screening and quality control (Giles et al., 2019).

3.1.4. ERA5 reanalysis data

In addition to the previous data sets, we employed daily meteorological/climatological data from the latest ERA5 reanalysis produced by the European Center for Medium-range Weather Forecasts (ECMWF) under the Copernicus Climate Change Service. Although the main reason for air pollution is the increase of pollutant concentration in the atmosphere, the local and regional meteorological/climatological conditions have also affected the air quality (Ghahremanloo et al., 2020; Kanniah et al., 2020; Nichol et al., 2020). Thus, in this study, we also investigated the relationship between satellite-derived air pollutants and ERA5's meteorological/climatological parameters, namely, the eastward-northward components of wind speed (WS), air temperature (Temp.), surface pressure (Pres.) and total precipitation (Prec.) with a spatial resolution of $0.25^{\circ} \times 0.25^{\circ}$.

3.1.5. Purchasing manager index data

The Purchasing Managers' Index (PMI) is one of the most important indicators of the economic activity that examines companies 'purchasing managers' tendency to purchase goods and services. It is one of the indices that can explain the growth forecasts of countries in the best way (Eren, 2014) (http://www.bireyselyatirimci.com/pmi-endeksi-nedir/). On the other hand, faster expansion in industrial activities or any reduction in PMI may cause to increase or decrease in air pollutants. Thus, we examined whether there was any correlation between PMI and satellite-derived pollutants. Besides, this analysis may explain if industrial activities have a high impact on air pollutants by expecting the pollutants should reduce in COVID-19 lockdown days.

3.2. Methodology

In this study, we focused on the following analyses: 1) monthly NO_2, SO_2 and AOD images and their statistics were extracted for 2019 and 2020.2) Hourly TROPOMI-based NO_2 values were compared with three station-based NO_2 in Istanbul. 3) The performance of MODIS AOD was validated using AOD from two ground-based stations. 4) The relationship between monthly average meteorological/climatological parameters and monthly average satellite-based pollutants was investigated. Finally, 5) The relationship between monthly average satellite-based pollutants and (PMI) was examined. Fig. 2 represents the workflow used to analyze pollutant concentration and related variables, which involve five source data sets, namely, (i) Sentinel-5P TROPOMI-based NO2 and SO2 products, and MODIS-based AOD product; (ii) meteorological parameters (e.g. Temp., Pres., Prec., WS) from ERA5, and (iii) AERONET AOD data, (iv) NO2 and SO2 ground measurements from TAQMS stations, and (v) PMI dataset. In this study, we used free image collection of TROPOMI and MODIS instruments in GEE datasets. GEE is an open-source geospatial analysis platform that enables users to globally or locally visualize and analyze changes, map trends, and quantify differences on the Earth's surface. Many studies related to land cover changes (Huang et al., 2017), crop mapping (Clemente et al., 2020), disaster management (DeVries et al., 2020), surface water change (Xia et al., 2019), and natural resource management (Aksoy et al., 2019; Leinonen et al., 2018) were carried out successfully and efficiently on the GEE platform. Concerning the analyses, a JavaScript program was developed in GEE to acquire, correct and visualize the data from image collections. The codes used in this paper can be found in the supplementary material. In this stage, the selected images are processed using the following steps:

(a) filtered the imaging time over the clipped region of interest (whole Turkey),
(b) removed cloudy pixels using a conditional (cloud_fraction >0.5) on TROPOMI-based products (Fioletov et al., 2020; Ialongo et al., 2020; Lorente et al., 2017, 2019; Van Geffen et al., 2018) and using best quality condition (for QA band AOD = 0) on MODIS-derived AOD data,

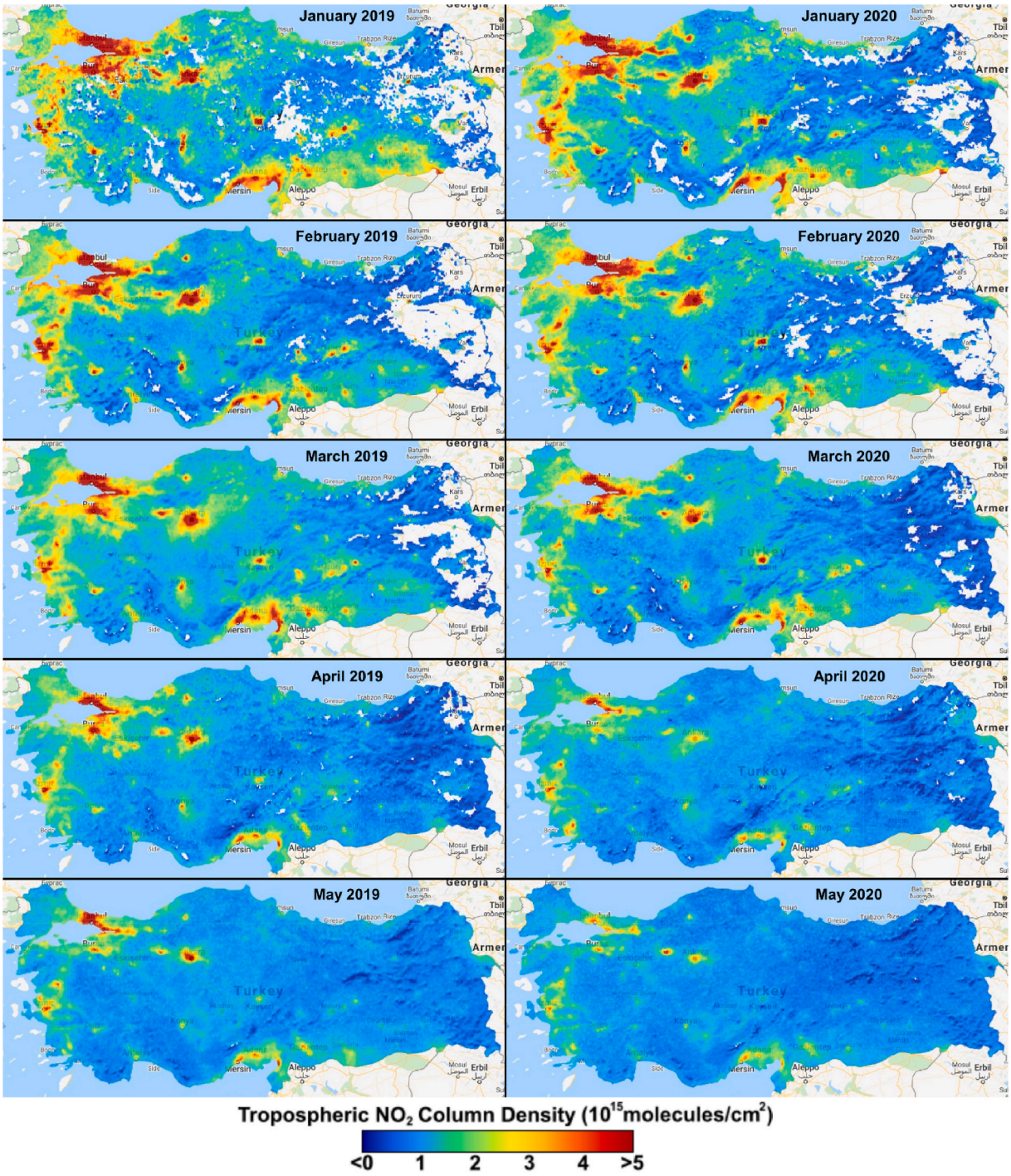

Fig. 3. The monthly images of tropospheric NO2 column density over Turkey.

(c) extracted daily images by mosaicking the overlapping scenes over the whole study zone,
(d) extracted hourly AOD pixel value, NO2 and SO2 column density pixel values from images covering the ground stations (TAQMS stations and AERONET sites) for the validation processes,
(e) calculated the monthly images by averaging the daily images for preparing monthly spatio-temporal maps and also for calculating the relationship between meteorological parameters in the lock-down months. Furthermore, for investigating the relationship between PMI and air pollutants.

Hourly data were only used for the validation step. TROPOMI-based NO2 and SO2 data were compared with TAQMS ground-measurements for three test sites (urban, urban-traffic and suburban) in the city of Istanbul. To evaluate MODIS AOD 470 nm data, we applied AERONET data (AOD440 and AOD500) with a time tolerance of ±0.5 h. Since AERONET does not provide AOD 470 nm, the mean value of AERONET AOD 440 nm and 500 nm values were calculated for AOD 470 nm retrieval relevant to MODIS AOD 470 nm (Equation (1)).

$$AOD\ (470nm) = \frac{AOD(500nm) + AOD(440nm)}{2} \quad (1)$$

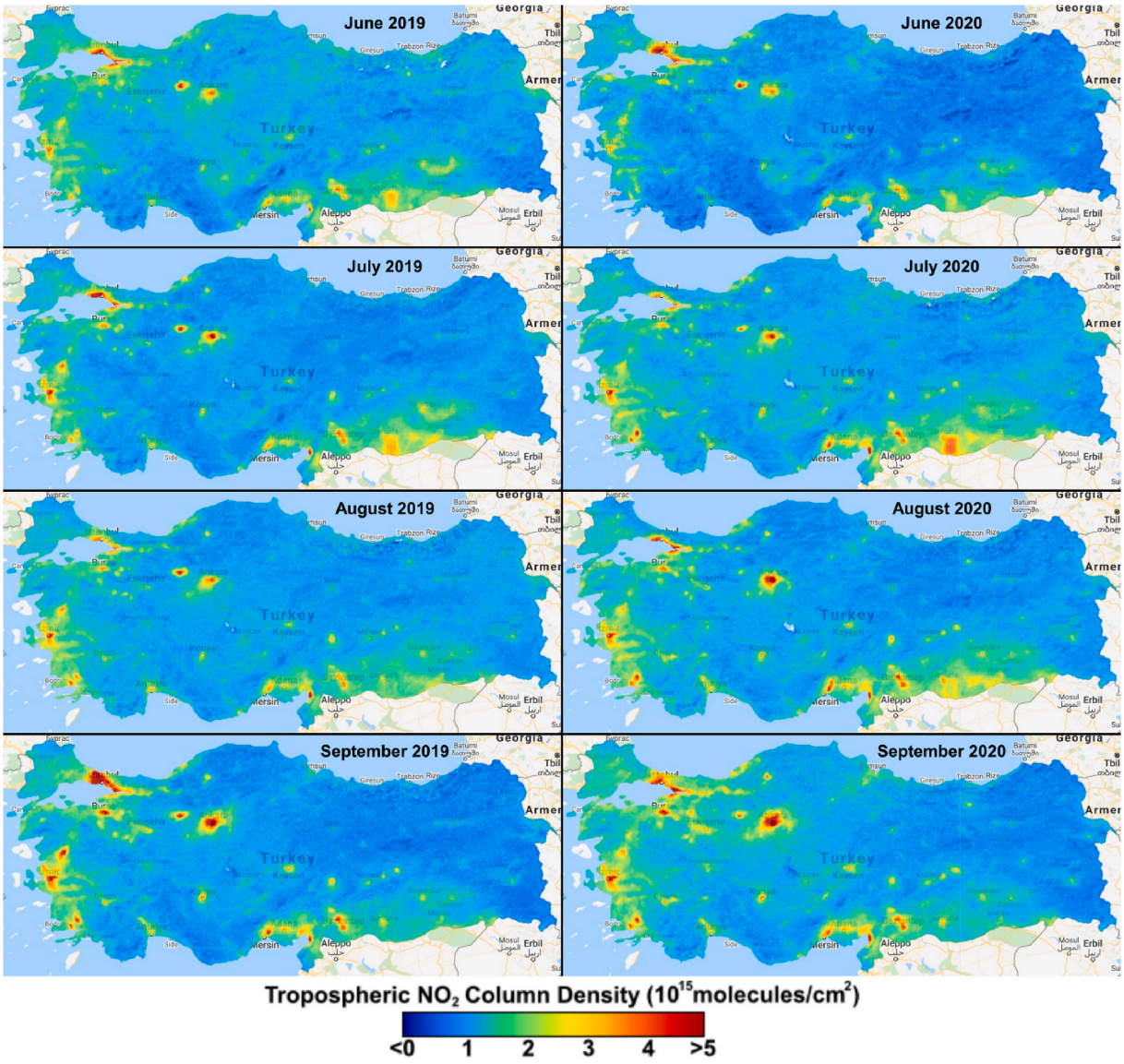

Fig. 3. (*continued*).

We utilized four statistical metrics below, namely, correlation coefficient (R), Root Mean Square Error (RMSE), Standard Deviation of Error (STD Error), and Bias to examine the relationship between MODIS AOD and AERONET AOD.

$$R = \frac{\sum\left(y_i - \overline{y}_i\right)\left(x_i - \overline{x}_i\right)}{\sqrt{\sum\left(y_i - \overline{y}_i\right)^2 \sum\left(x_i - \overline{x}_i\right)^2}} \tag{2}$$

$$RMSE = \sqrt{\frac{\sum\left(x_i - y_i\right)^2}{n}} \tag{3}$$

$$SDT\ of\ Error = \sqrt{\frac{\sum\left(y_{Error} - \overline{y_{Error}}\right)^2}{n}} \tag{4}$$

$$Bias = \frac{\sum\left(x_i - y_i\right)}{n} \tag{5}$$

Where y_i, x_i, $\overline{y}_i$, and $\overline{x}_i$ are the MODIS-derived AOD, AERONET-based AOD, their mean values, respectively. Thus, y_{Error} refers to the difference between MODIS-derived AOD and AERONET-based AOD, and $\overline{y_{Error}}$ refers to the mean of differences.

In the last stage, to investigate if the meteorological/climatological parameters play an important role in the results of pollutants in the lockdown period, the monthly meteorological data of ERA5 with the selected information layer were used to extract the correlation coefficients. Furthermore, the relationship between monthly pollutants and PMI was also investigated to find out the effect of PMI on pollutants.

To summary the innovation in the methodology; i) a JavaScript program in the GEE was developed to automate the image analysis, ii) satellite-based pollutants were compared and analyzed with ground based observations from different land cover types, iii) the relationship between meteorological parameters/PMI and satellite-based pollutants was analyzed.

4. Results and discussion

4.1. Spatio-temporal distribution of tropospheric NO_2 column density over Turkey

The lockdown in Turkey due to the outbreak of COVID-19, mainly from March 10, 2020 to May 31, 2020, decreased transportation

Table 2
Average, standard deviation, maximum, minimum, and percentage of change rate values of the TROPOMI NO2 column density calculated during January–September 2019 and 2020 over Turkey.

Month	Jan.		Feb.		Mar.	
Year	2019	2020	2019	2020	2019	2020
Average	1.6581	1.5213	1.4235	1.3764	1.4557	1.2148
S.D	1.0930	1.1745	1.1187	0.9953	0.8698	0.7736
Min	−1.4851	−2.1240	−1.4960	−1.0804	−0.7089	−1.0800
Max	13.1696	18.6903	39.3789	22.9577	12.4227	9.7954
Area (km^2) for NO_2>4	23800.3	23509.2	18291.8	16129.8	13388.6	9027.1
PCR	−8.25		−3.31		−16.55	
Month	Apr.		May		Jun.	
Year	2019	2020	2019	2020	2019	2020
Average	1.1364	1.0129	1.0530	0.9214	1.2372	1.0076
S.D	0.7060	0.4808	0.5037	0.3791	0.3785	0.3999
Min	−0.6486	−1.3173	−0.6213	−0.8127	−0.6144	−0.5564
Max	12.5657	6.2744	9.1033	5.9866	7.5727	6.5480
Area (km^2) for NO_2>4	5733.7	1644.4	3476.6	356.1	808.2	903.8
PCR	−10.86		−12.49		−18.56	
Month	Jul.		Aug.		Sep.	
Year	2019	2020	2019	2020	2019	2020
Average	1.1591	1.2772	1.2227	1.2437	1.1642	1.2789
S.D	0.4211	0.4093	0.3626	0.4532	0.5225	0.5005
Min	−0.4497	−0.2739	0.0937	0.1062	0.0304	0.2295
Max	6.8161	7.9473	7.7835	7.2345	7.2871	7.4934
Area (km^2) for NO_2>4	1270.2	1689.8	618.6	1920.0	4225.0	3246.3
PCR	10.19		1.71		9.85	

activities that lead to lower energy consumptions and less oil request. Moreover, it provided a good opportunity to study its impacts on air quality by comparing some pollutant concentrations. Although there are many key parameters that may change the air pollution concentration, this study is conducted based on the assumption of the used parameters and corresponding analyses. One of the important trace gases in the atmosphere is NO_2. While some nitrogen oxides naturally occur, some of them are due to human activities. The major part of NO_2 produced by human activities is related to the burning of fuel in stationary sources and resulting from combustion in vehicles and industrial enterprises (Ghahremanloo et al., 2020; Kanniah et al., 2020).

Fig. 3 shows the monthly comparisons of spatial tropospheric NO_2 images over Turkey from January 2019 to September 2020. There are no-data pixels in the east-direction of images such as January and February that result from cloudy pixel conditions and quality assurance (QA) limitation of the algorithms (Ialongo et al., 2020; Lorente et al., 2017; Nichol et al., 2020; Omrani et al., 2020; Zheng et al., 2019). As seen in Fig. 3, these images display a general reduction in NO_2 distribution when comparing January–Jun 2019 with January–June 2020. In particular, the spatial distribution of NO_2 decreased significantly during the lockdown period (March–May 2020) compared to the same period of 2019. In order to support these visual interpretations, the area information in Table 2, where $NO_2 > 4*10^{15}$ molec/cm^2, was extracted. The area information from January to June 2019 varied from 23800.3 km^2 to 3476.6 km^2, respectively, whereas it ranged from 23509.2 km^2 to 356.1 km^2 for the same period of 2020. However, after the lockdown restrictions are relaxed in July, the NO_2 concentration started to increase in July, August and September 2020 compared to the same months of 2019. The area information in Table 2 also reveals this increase. This observable increase was probably due to the rising vehicle emissions and industrial activities after the lockdown period. The tropospheric NO_2 reduction obtained during the lockdown period in Turkey coincides with similar studies conducted over different countries (Fan et al., 2020; Mesas-Carrascosa et al., 2020; Metya et al., 2020; Nichol et al., 2020; Tobías et al., 2020; Vîrghileanu et al., 2020).

Concerning the general evaluation of the spatial variability of NO_2 pollution over Turkey, Marmara and Aegean regions show the highest spatial variability of NO_2, whereas the Mediterranean, Southeastern Anatolia, and central Anatolia partly revealed high NO_2 distribution.

In addition to the spatio-temporal comparisons of 2019 and 2020 images, it would be better to provide quantitative analyses for this period as in Fig. 4 and Table 2. Fig. 4 reveals the monthly average TROPOMI-based NO_2 column density over Turkey in 2019 and 2020. As a general evaluation, the trend of monthly NO_2 averages shows the

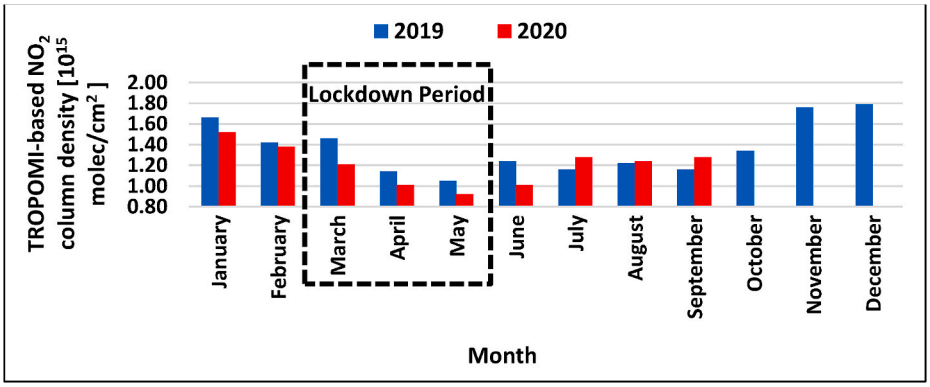

Fig. 4. The monthly average TROPOMI-based NO_2 column density over Turkey in 2019 and 2020.

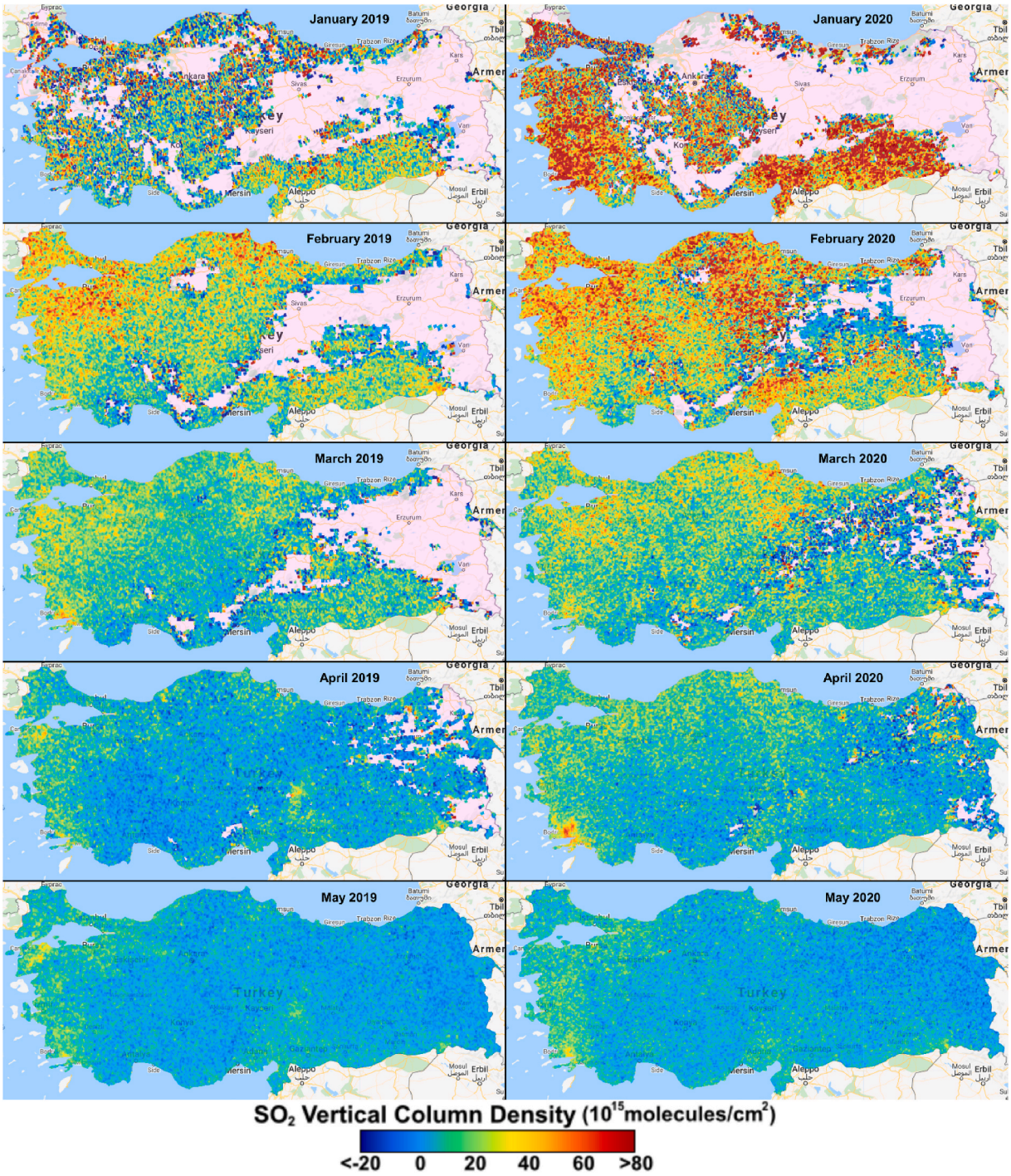

Fig. 5. The monthly images of SO2 column density over Turkey.

maximum amount in the winter, while the minimum amount in the summer. In Fig. 4, a decrease was observed in monthly average NO_2 values from January to July in 2020, and these values were also lower than 2019 monthly averages. Considering the lockdown period, the monthly average NO_2 values declined in 2020 compared to the same period of 2019. On the other hand, after the lockdown period, the monthly average NO_2 values increased dramatically in 2020, which were also higher than in 2019. Table 2 shows the results of the statistical parameters, namely, average, standard deviation (S.D), minimum (min), maximum (max), and percent of change rates (PCR) obtained from the monthly NO_2 images. The average value of NO_2 column density dropped from $1.66*10^{15}$ molec/cm^2 to $1.05*10^{15}$ molec/cm^2 from January to June, and then increased to $1.79*10^{15}$ molec/cm^2 in December in 2019. On the other hand, in 2020, the average NO_2 values started from $1.52*10^{15}$ molec/cm^2 in January, then slightly decreased to $0.92*10^{15}$ molec/cm^2 in May, and finally reached $1.28*10^{15}$ molec/cm^2 in September. The statistical results in Table 2 demonstrate that a descending trend was observed in 2020 in comparison with 2019. In addition, the monthly PCR between 2019 and 2020 for March, April, May and June were calculated as −16.5%, −10.8%, −12.49% and −18.56%, respectively, proving the descending trend in the lockdown. It is obvious that the lockdown of the COVID-19 outbreak and staying at

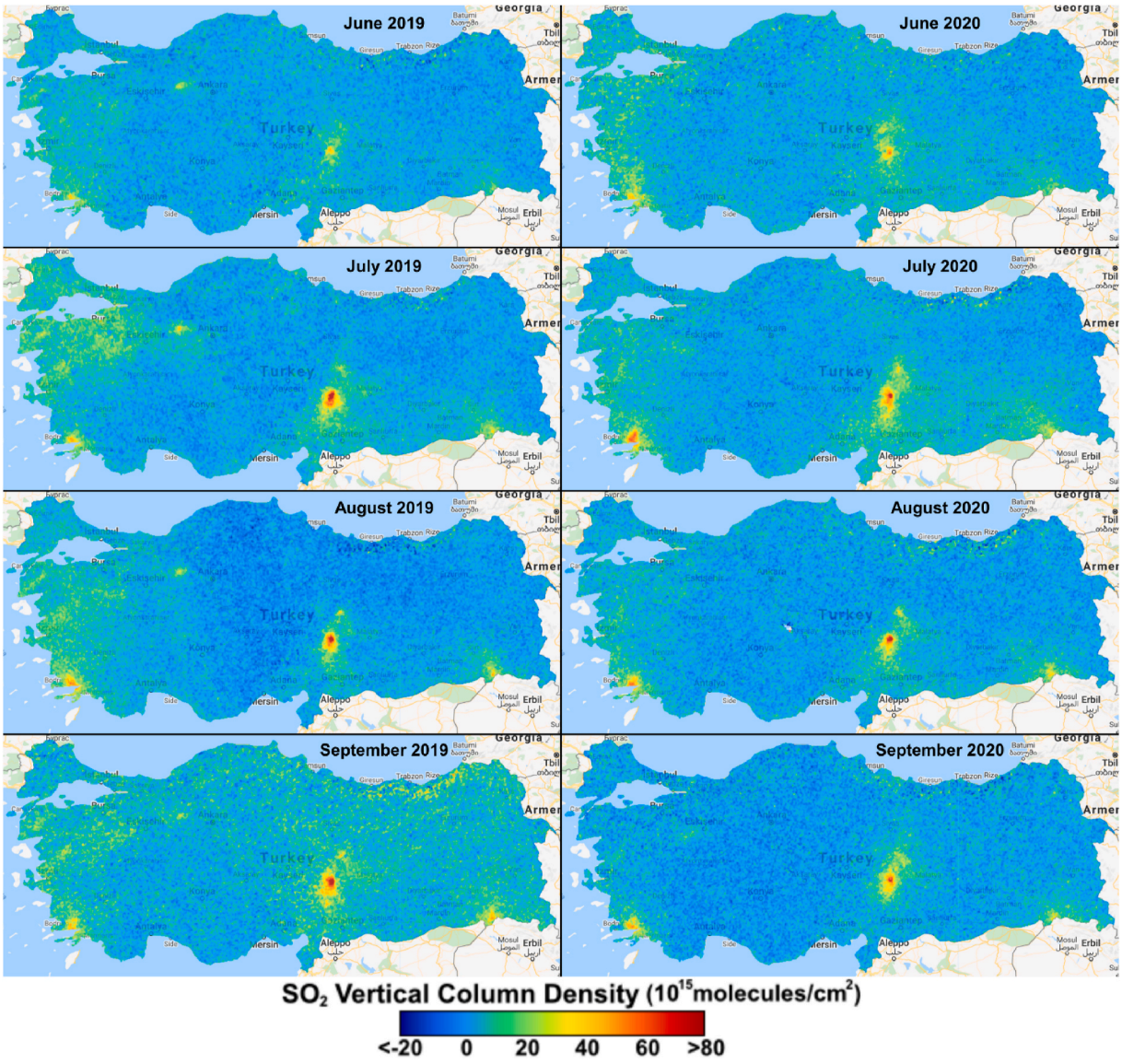

Fig. 5. (*continued*).

home have caused a significant reduction in tropospheric NO_2 column density.

4.2. Spatio-temporal distribution of SO_2 column density over Turkey

SO_2 is one of the tropospheric trace gases that is mostly produced by volcanoes and industrial activities. Due to the presence of sulfur compounds in oil and coal, their combustion leads to the production of SO_2. We analyzed the spatio-temporal variations of the monthly average SO_2 column density over Turkey as in Fig. 5. No-data pixels are available from January to April in both 2019 and 2020 data sets. The main reasons are cloud fraction condition, the algorithm limitations for producing the data and quality assurance contrast. Due to noise on the SO_2 values, negative vertical column concentrations are perceived as low SO_2 emissions. According to the Sentinel-5P product readme file (https://sentinel.esa.int/web/sentinel/technical-guides/sentinel-5p/products-algorithms), it is recommended to filter outliers as concentration values lower than -0.001 mol/m^2.

Since the number of no-data pixels is too many in Fig. 5 for January, February and March of 2019 and 2020 images, the proper comparison is not possible for these months. However, concerning the concentrations of SO_2 values in these months, 2020 datasets had significantly higher concentrations than 2019. The area information in Table 3, where $SO_2 > 60*10^{15}$ molec/cm^2, was extracted to observe the areal changes. The area information from January to September 2019 varied from 38167.5 km^2 to 307.9 km^2, respectively, while it ranged from 152073.3 km^2 to 317.0 km^2 for the same period of 2020. In 2020, the area information of September image was the only image that showed less area than in 2019. The lockdown months, except March, showed no significant decrease compared to 2019. On the contrary, the spatial distribution of SO_2 values in the 2020 lockdown period had slightly higher concentrations than the same period of 2019. These results revealed that the lockdown had no effect on reducing the pollution caused by SO_2. On the other hand, after the lockdown restrictions are relaxed in July, the monthly SO_2 distributions were identical for the following months in both 2019 and 2020. Concerning the literature, some studies also revealed similar results as in our study that the column density of SO_2 remained unchanged or increased in some regions of the related countries (Ghahremanloo et al., 2020; Tobías et al., 2020).

Fig. 6 represents the monthly average TROPOMI-based SO_2 column density over Turkey in 2019 and 2020. As a general evaluation, the trend of monthly SO_2 averages shows the maximum amount in the winter,

Table 3
Average, standard deviation, maximum, minimum, and percentage of change rate values of the TROPOMI SO_2 column density calculated during January–September 2019 and 2020 over Turkey.

Month	Jan.		Feb.		Mar.	
Year	2019	2020	2019	2020	2019	2020
Average	17.7540	50.4978	23.5050	33.1631	13.8294	15.9301
S.D	32.2796	52.6739	20.4712	31.2283	13.8729	17.9774
Min	−60.2049	−60.2131	−60.2036	−60.1869	−59.9939	−60.1687
Max	378.6225	971.4098	618.0464	628.6281	284.0248	455.0226
Area(km^2) for SO_2 > 60	38167.5	152073.3	22561.5	93253.3	2661.4	8845.8
PCR	184.43		41.09		15.19	
Month	Apr.		May		Jun.	
Year	2019	2020	2019	2020	2019	2020
Average	5.3751	9.3876	4.4431	4.9014	3.4746	4.7309
S.D	9.9822	11.5643	6.3090	7.0158	4.8672	5.7577
Min	−55.6041	−59.8140	−24.3164	−27.1609	−31.1326	−21.0456
Max	190.2	287.1	56.1	187.7	54.7	70.2
Area (km^2) for SO_2>60	978.1	2149.7	0.0	54.8	0.0	19.4
PCR	74.65		10.31		36.16	
Month	Jul.		Aug.		Sep.	
Year	2019	2020	2019	2020	2019	2020
Average	4.4094	4.6210	2.7875	3.2505	7.2199	2.4038
S.D	6.4622	6.2672	6.6889	6.0039	6.9321	6.2358
Min	−19.2326	−32.0067	−41.5177	−46.8179	−29.2360	−28.8736
Max	108.5817	111.0524	101.9469	108.5692	109.0529	92.9221
Area (km^2) for SO_2>60	523.5	410.3	307.9	317.0	486.8	176.5
PCR	4.80		16.61		−66.71	

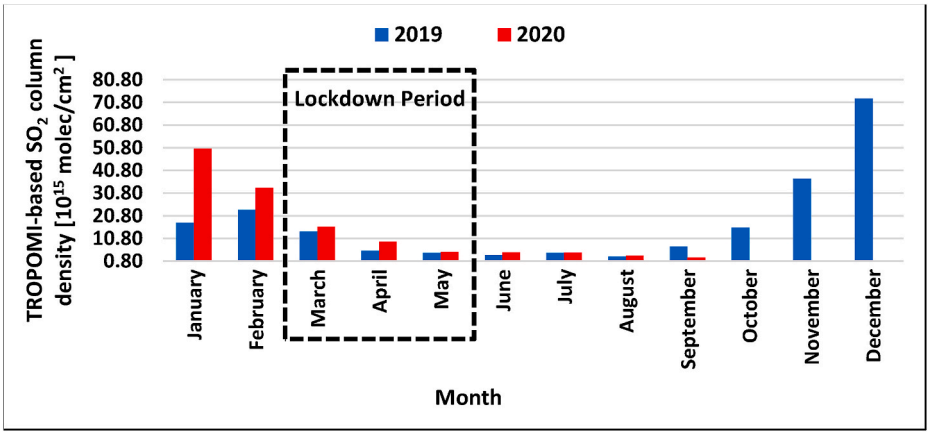

Fig. 6. The monthly TROPOMI-based SO_2 column density over Turkey in 2019 and 2020.

while the minimum amount in the summer. In Fig. 6, a decrease was observed in monthly average SO_2 values from January to September in 2020, and these values were close to or higher than 2019 monthly averages. Concerning the lockdown period, the monthly average SO_2 values were slightly higher in 2020 compared to the same period of 2019. Table 3 provides the results of the statistical parameters, namely, average, S. D, min, max and PCR obtained from the monthly SO_2 images. The average value of SO_2 column density dropped from $23.51*10^{15}$ molec/cm^2 to $3.48*10^{15}$ molec/cm^2 from February to July, and then increased to $72.46*10^{15}$ molec/cm^2 in December 2019. On the other hand, in 2020, the average SO_2 values started from $50.50*10^{15}$ molec/cm^2 in January, then slightly decreased to $2.40*10^{15}$ molec/cm^2 in September. The statistical results in Table 3 (average and PCR) demonstrate that an ascending trend was observed when comparing 2020 with 2019. The only negative monthly average SO2 trend between 2020 and 2019 was observed in September as −66.71%. The results of the monthly average SO2 values showed that the lockdown of COVID-19 outbreak and staying at home had no significant reduction on tropospheric SO2 column density.

4.3. Spatio-temporal distribution of MODIS-based AOD over Turkey

Aerosols are suspensions of solid particles or liquid droplets in a gas, and they generally refer to dust particles such as ash, mist, smog, etc. Human-made aerosols are commonly found near large human habitats. The telemetry parameter used in this connection is the optical depth of the atmosphere. The aerosol optical depth (AOD) index is a measure of an aerosol that is calculated based on the ratio of solar waves propagated and absorbed in the atmosphere along the wavelength and the path traveled. This index is a quantitative parameter to indicate the density and concentration of particles in the atmosphere and is generally calculated along a vertical path (Filonchyk and Yan, 2019; Wei et al., 2019).

In order to provide the best quality AOD data, masking operation was applied to the AOD Quality Assessment (AOD_QA) band for generating monthly AOD images in Fig. 7. Although the number of no-data pixels is too many in Fig. 7 for January, February, March and April, proper comparison can be made since the spatial presence of the AOD data are identical in both 2019 and 2020 images. Concerning the spatial distribution of AOD in January and February 2020 images have lower AOD

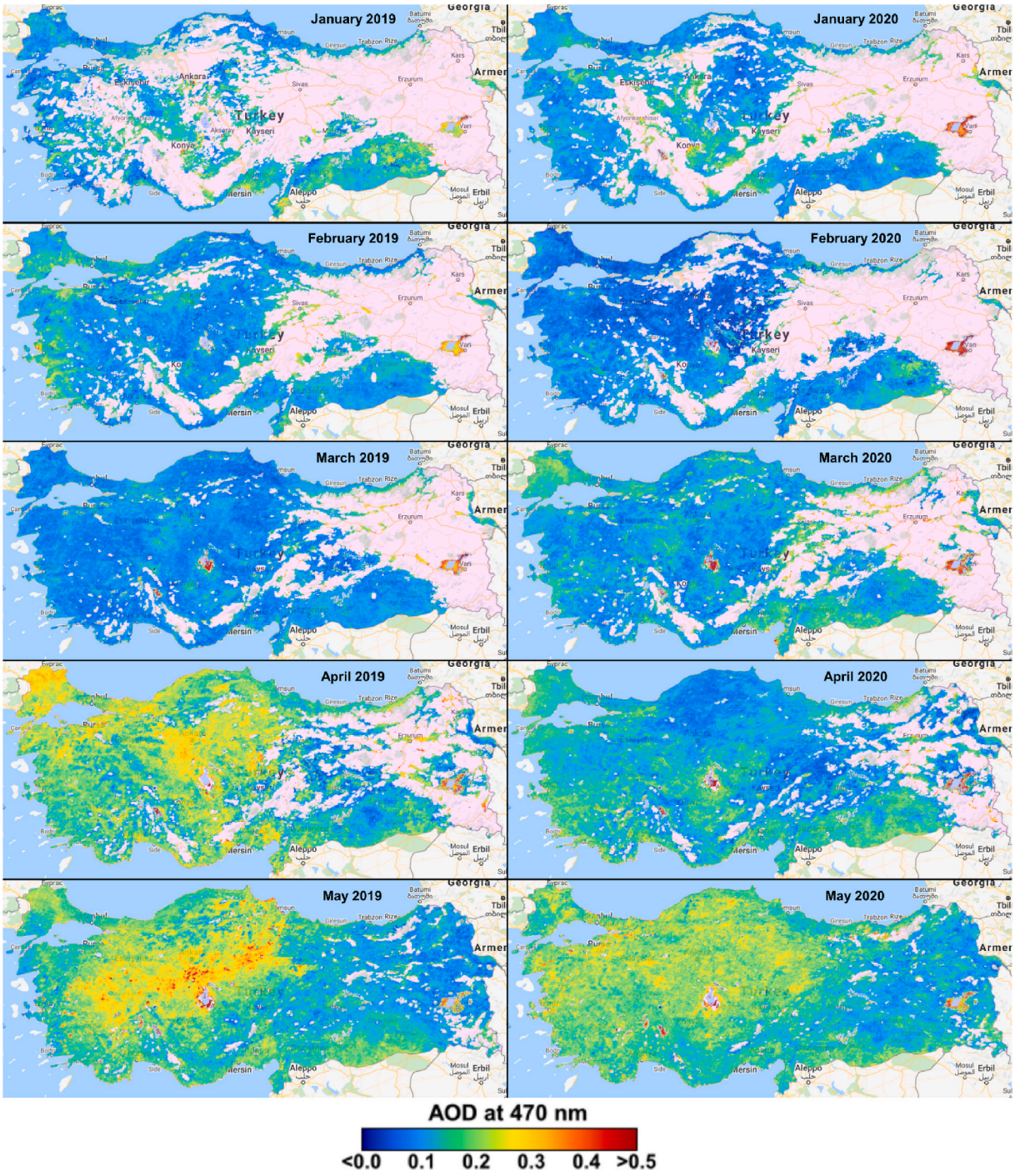

Fig. 7. The monthly images of MODIS-derived AOD concentration over Turkey.

concentration than 2019 images. However, in March, the AOD distribution is higher in 2020 compared to the 2019 image. In the following lockdown month, April, a significant decrease in monthly AOD distribution was observed in 2020 compared to the same month of 2019, indicating the effect of lockdown was significant on AOD reduction. Since April 2020 was the month with the tightest restrictions. In the last month of lockdown (May 2020) and June 2020, almost identical AOD distribution was observed as in May–June 2019, while the density of AOD distributions varied from region to region. After the lockdown period, the monthly AOD distribution was higher in July 2020 and September 2020, whereas lower in August 2020 compared to the same months of 2019. On the other hand, the area information in Table 4, where AOD >0.4, was extracted to observe the areal changes. The area information from January to April 2019 varied from 394.6 km^2 to 1026.8 km^2, respectively, while it ranged from 722.4 km^2 to 2121.9 km^2 for the same period of 2020. Then, from April 2019 to July 2019, the area information was between 1616.5 km^2 and 1223.1 km^2, respectively, which was higher than the same period of 2020 (940.2–820.5 km^2). After the restrictions were relaxed in June, the area information of July, August and September 2020 was higher than the same months of 2019. The results of some studies also supported our findings by showing a decreasing trend in AOD in different test sites during the lockdown

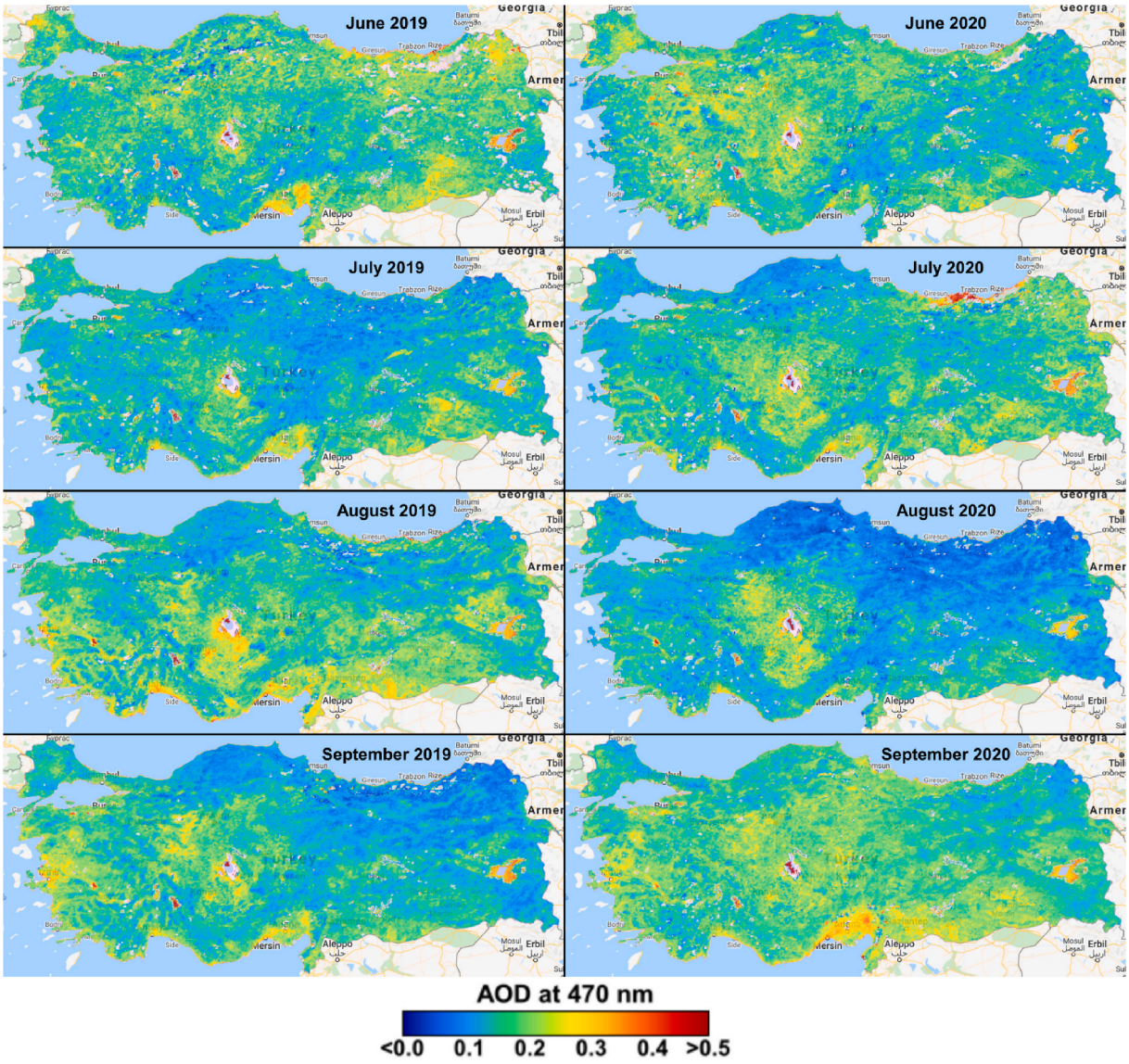

Fig. 7. (*continued*).

period (Ghahremanloo et al., 2020; Kanniah et al., 2020; Otmani et al., 2020).

Fig. 8 and Table 4 present comparative and quantitative statistical results of monthly AOD values over the study area for both 2019 and 2020. As a general evaluation of Fig. 8, the trend of monthly AOD averages from April to October is higher than the yearly averages, while the rest of the months reveal lower monthly average AOD than the yearly average. The monthly average AOD values in Fig. 8 coincided with the results of the spatio-temporal analysis presented above. We can see a significant decrease in April 2020 compared to April 2019. Besides, a sharp increase from 0.096 in March 2019 to 0.0186 in April 2019 can be seen clearly in the spatial distribution map in Fig. 7. In 2020, the lowest and highest values ranged from 0.096 to 0.186 in February and September, respectively. The statistical results of monthly AOD images in Table 4 display the PCR about −29.84% in April and 20.62% in September considering the comparison between 2019 and 2020.

4.4. Quantitative analysis of TROPOMI-based and station-based NO_2 and SO_2 for three test sites

This quantitative analysis relies on geostatistical data processing of the collected data including TROPOMI-based NO_2 column density (molec/cm^2), TROPOMI-based SO_2 vertical column density, related and ground station-based NO_2 concentrations (μg/cm^3). In Istanbul, we selected the statistical data from three ground stations (Fig. 1) as traffic-urban (Beşiktaş(, urban (Başakşehir), and suburban (Şile) stations. The monthly trendlines revealed the decrease in the tropospheric NO_2 column density from January to September for all selected hotspots (Fig. 9a–c) in 2019 and 2020. Furthermore, the ground station measurements also confirmed this downward trendline in 2019 and 2020 for all test sites (Fig. 9d–f). In the suburban location, due to no data in February (Fig. 9c), we could not calculate the satellite image data for 2019 and 2020. The other important outcome of this analysis was that the monthly NO_2 levels were higher in 2019 than 2020 for all three sites and both data sets. In the suburban site, TROPOMI-based NO_2 (Fig. 9c) and station-based NO_2 (Fig. 9f) showed identical behavior in 2019 and 2020. However, in the urban test sites, the difference between 2019 and 2020, especially in the lockdown months (March–May), are obviously seen for both datasets (Fig. 9a–b and Fig. 9d–e). As in the NO_2 results, a decreasing trend in the SO_2 column density was observed from January to September for all selected hotspots (Fig. 9g–i) in 2019 and 2020. However, the ground station-based SO_2 provided opposite trends in 2019 and 2020 for urban and suburban test sites (Fig. 9j-l). In these sites, the ground-based SO_2 concentration has an increasing trend in 2020,

Table 4
Average, standard deviation, maximum, minimum, and percentage of change rate values of the MODIS-derived AOD calculated during January–December 2019 and 2020 over Turkey.

Month	Jan.		Feb.		Mar.	
Year	2019	2020	2019	2020	2019	2020
Mean	0.1298	0.1155	0.1155	0.0889	0.0955	0.1245
S.D	0.0484	0.0447	0.0429	0.0459	0.0407	0.0494
Min	0.0000	0.0000	0.0000	0.0000	0.0000	0.0000
Max	0.6040	2.1270	0.5980	1.1300	1.4710	0.8880
Area (km^2) for AOD>0.4	394.6	722.4	426.0	1191.3	1026.8	2121.9
PCR	−10.98		−23.07		30.32	
Month	Apr.		May		Jun.	
Year	2019	2020	2019	2020	2019	2020
Mean	0.1859	0.1304	0.1757	0.1761	0.1736	0.1652
S.D	0.0636	0.0517	0.0761	0.0568	0.0765	0.0680
Min	0.0000	0.0000	0.0000	0.0000	0.0000	0.0000
Max	1.1970	4.0000	4.0000	4.0000	4.0000	4.0000
Area (km^2) for AOD>0.4	1616.5	940.2	4262.5	1467.8	1223.1	820.5
PCR	−29.84		0.24		−4.80	
Month	Jul.		Aug.		Sep.	
Year	2019	2020	2019	2020	2019	2020
Mean	0.1444	0.1622	0.1695	0.1283	0.1514	0.1826
S.D	0.0619	0.0854	0.0712	0.0897	0.0700	0.0946
Min	0.0000	0.0000	0.0000	0.0000	0.0000	0.0000
Max	4.0000	4.0000	4.0000	4.0000	4.0000	4.0000
Area (km^2) for AOD>0.4	378.0	1728.6	930.9	514.5	748.6	1050.4
PCR	12.38		−24.34		20.62	

while a decreasing trend is observed in 2019, showing that the lockdown restrictions were not effective in decreasing the ground-based SO_2 levels as in the satellite-based results.

Indeed, TROPOMI-based NO_2 and SO_2, and station-based measurements do not present the same quantity of NO_2 and SO_2, since the TROPOMI measures the total vertical amount of atmospheric NO_2 and SO_2, whereas ground stations provide only near-surface distribution of these pollutants. Even so, we checked if these data sets (satellite and ground measurements) have any relationship in this case study. In order to validate the TROPOMI-based vertical column product, it is required to have information on the vertical profile of the pollutant from the ground stations or other airborne systems. Concerning the total column of a pollutant, the vertical sensitivity of the retrieval is described by the total column-averaging kernel (Borsdorff et al., 2014). However, when the ground measurement is not a vertical profile, the application of the total column-averaging kernel becomes more difficult (Borsdorff et al., 2018). Only few ground stations are operational for providing the vertical profile of air pollutants over the world. The Total Carbon Column Observing Network (TCCON) and The Infrared Working Group (IRWG), having ground-based solar Fourier-transform spectrometers (FTS), are critical networks that provide regular ground-based measurements of the vertically integrated column amounts of some trace gases (Landgraf et al., 2018). Even so, some researchers claimed that they obtained from medium to high correlation coefficients between satellite and ground-based NO_2 measurements (Cersosimo et al., 2020; Pinardi et al., 2018; Vîrghileanu et al., 2020). In these studies, Vîrghileanu et al. (2020) had the correlation coefficients ranging from 0.597 to 0.865, and the correlation coefficients from the study of Cersosimo et al. (2020) varied between 0.50 and 0.90. Moreover, Pinardi et al. (2018) provided very good coherence for daily and monthly comparisons between TROPOMI tropospheric NO_2 vertical column density and ground-based NO_2 data about R equal to 0.89. Besides, some other experiments also revealed that the satellite-based NO_2 column density had a strong correlation with ground-based station data with a correlation coefficient almost above 0.8 (Bucsela et al., 2008; Huijnen et al., 2009; Kramer et al., 2008). Therefore, we also compared the TROPOMI-based NO_2 and SO_2 with ground-based measurements in three test sites (urban, urban-traffic and suburban) in Istanbul, and we obtained the correlation coefficients between 0.65 and 0.83 for NO_2, which coincide with the results of the above-mentioned studies. However, the SO_2 analyses did not respond well with R-value ranging from 0.004 to 0.15.

Considering the relationship between satellite-based and ground-based measurements, we applied the hourly measurement with a time shift of about ±30 min from January 1, 2019 to September 30, 2020 in three test sites. The NO_2 results in Fig. 10 illustrate the correlation coefficients of 0.83, 0.70, and 0.65 that were obtained from suburban (Fig. 10a), urban (Fig. 10b), and urban traffic stations (Fig. 10c), respectively. On the other hand, the SO_2 results in Fig. 10 reveal the correlation coefficients of 0.15, 0.004, and 0.014 that were obtained from suburban (Fig. 10d), urban (Fig. 10e), and urban traffic stations (Fig. 10f), respectively. These results showed that the more the ground-based NO_2 concentration was observed, the lower the correlation coefficient was obtained between satellite column density and ground-based measurements. Concerning the SO_2 comparisons, no significant relationship was found between satellite-based and ground-based measurements.

4.5. Validation of MODIS-Derived AOD and AERONET AOD

We have considered the AERONET AOD hourly data as reference data for validating the MODIS-derived AOD 470 nm. There are five AERONET sites over turkey, while two of them are appropriate in this study due to the time interval considered. First, because of lack of enough corresponding image data over the mentioned AERONET sites,

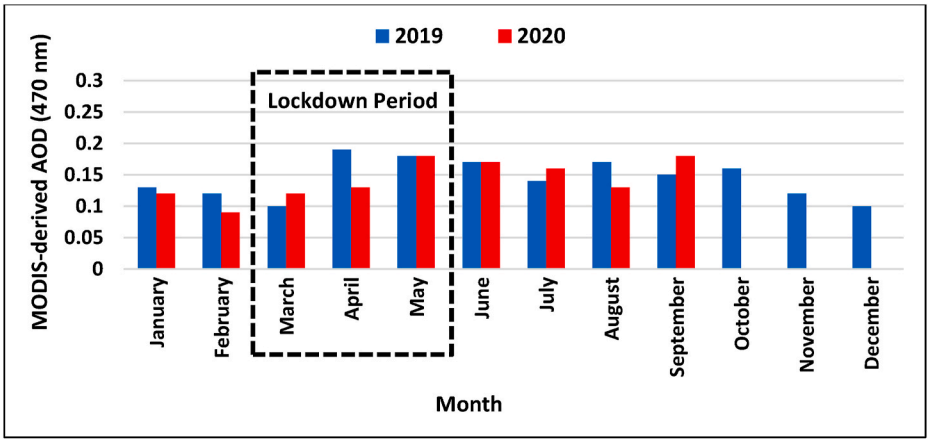

Fig. 8. The monthly average MODIS-derived AOD over Turkey in 2019 and 2020.

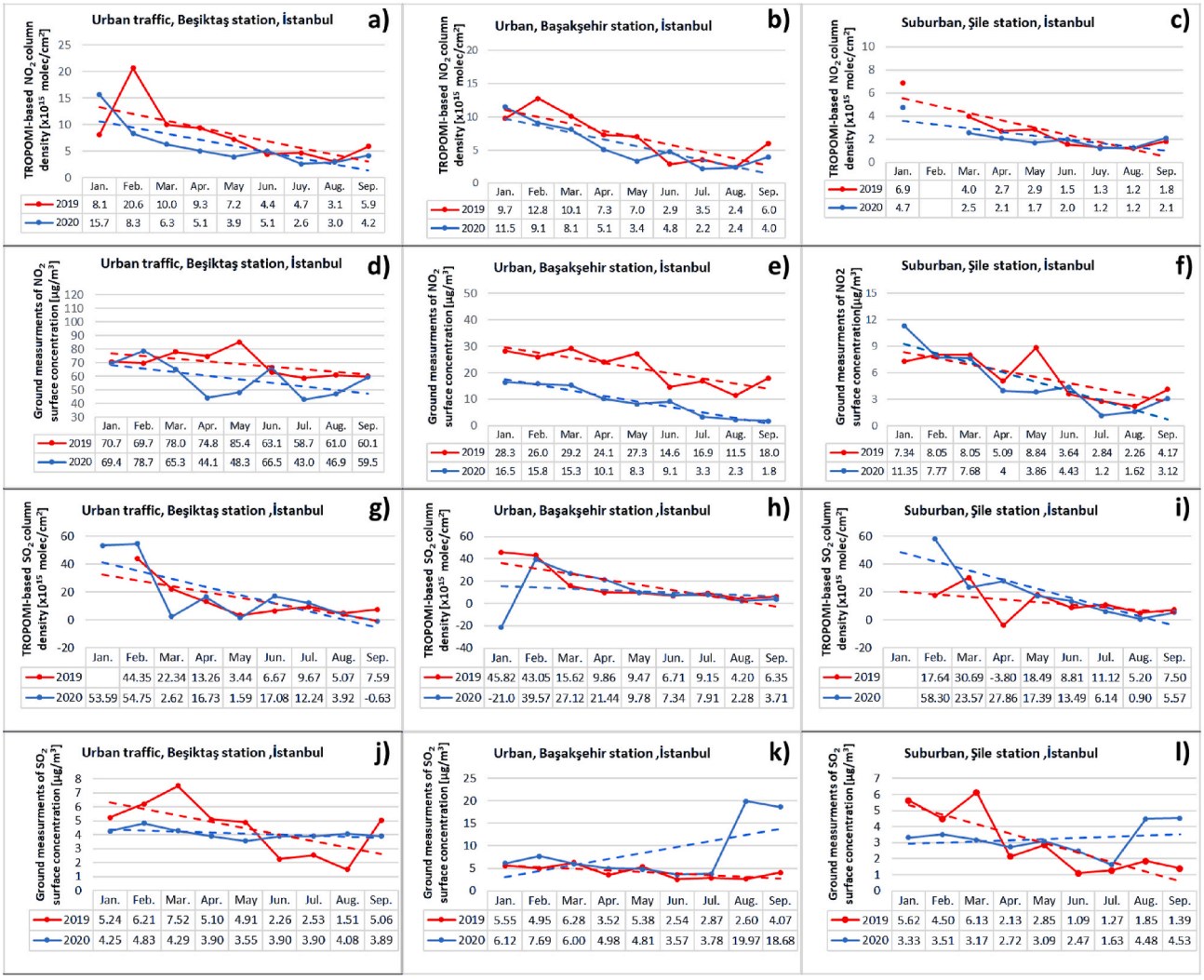

Fig. 9. Comparative graphs of the monthly TROPOMI-based NO_2 (a–c) and SO_2 (g–i) with ground-based measurements (d–f, j-l) for three stations between January and September in 2019 and 2020.

we used a distance buffer around sites almost 1.5 km and 6 km on ERDEMLI site and TUZ_GÖLÜ_3 site, respectively (henceforth mentioned with ERDEMLI* and TUZ_GÖLÜ_3*). Due to the absence of AERONET data in Tuz_Gölü_3* site, only July–August 2018 data sets were used for this site, whereas, for the ERDEMLI* site, the data were available from July 2018 to March 2019. The results of the validation analysis between MODIS-derived AOD and AERONET-based AOD are illustrated in Fig. 11. The findings show that MODIS-derived AOD is well correlated with the AERONET AOD in both ERDEMLI* and TUZ_GÖLÜ_3* sites with the R-value equal to 0.86 and 0.82, and RMSE equal to 0.065 and 0.097, respectively. According to some studies, these correlation coefficient values are much similar with other resulted thought varies methods (Aldabash et al., 2020; Zhang et al., 2020b). It is also worth noting that estimated surface reflectance's errors and AOD conversion algorithms in aerosol loading can be influence over obtained results (Grey et al., 2006; Gupta et al., 2016).

4.6. Relationships between monthly average satellite-based air pollutants and climatological/meteorological parameters

It is worth emphasizing that the air quality does not depend only on the concentration of the pollutants, but also on the local and regional climatological and meteorological conditions (Ji et al., 2020). Researchers have investigated the spatial and temporal relationship between air pollutants and key meteorological factors (Athanassiadou et al., 2010; Banerjee et al., 2011). In addition, some studies have shown that meteorological conditions controlled the spatial and temporal impacts on air quality (Ji et al., 2020; Qiao et al., 2019). Hence, these factors and parameters should be thoroughly investigated to find out the impact of human and industrial activities on the pollutant concentration in the atmosphere. Therefore, we examined the correlation between each pollutant and key meteorological/climatological parameters for the lockdown period. Meteorological/climatological parameters include the monthly average of air temperature (Temp.) from the ground to 2 m height in Kelvin, the monthly sum of total precipitation (Prec.) in meters, the monthly average of Surface pressure (Pres.) in pascal, and the monthly average of wind speed (WS) in 10 m of ground in m/s. Table 5 provides the monthly average values of all parameters and the correlation coefficients between them. Table 5 shows significant correlations between all pollutants and air temperature in 2019 and 2020 ranging from 0.68 to 0.98. While the air temperature revealed strong negative correlations with NO_2 and SO_2, it had a high positive correlation with AOD for the lockdown period. Concerning the surface pressure, the correlations with all pollutants showed identical behaviors as in air temperature providing negative correlations with NO_2 and SO_2, whereas positive correlation with AOD. Besides, the absolute value of these correlations varied from 0.55 to 0.99 in 2019 and 2020. The precipitation and air pollutants did not have high correlations presenting almost

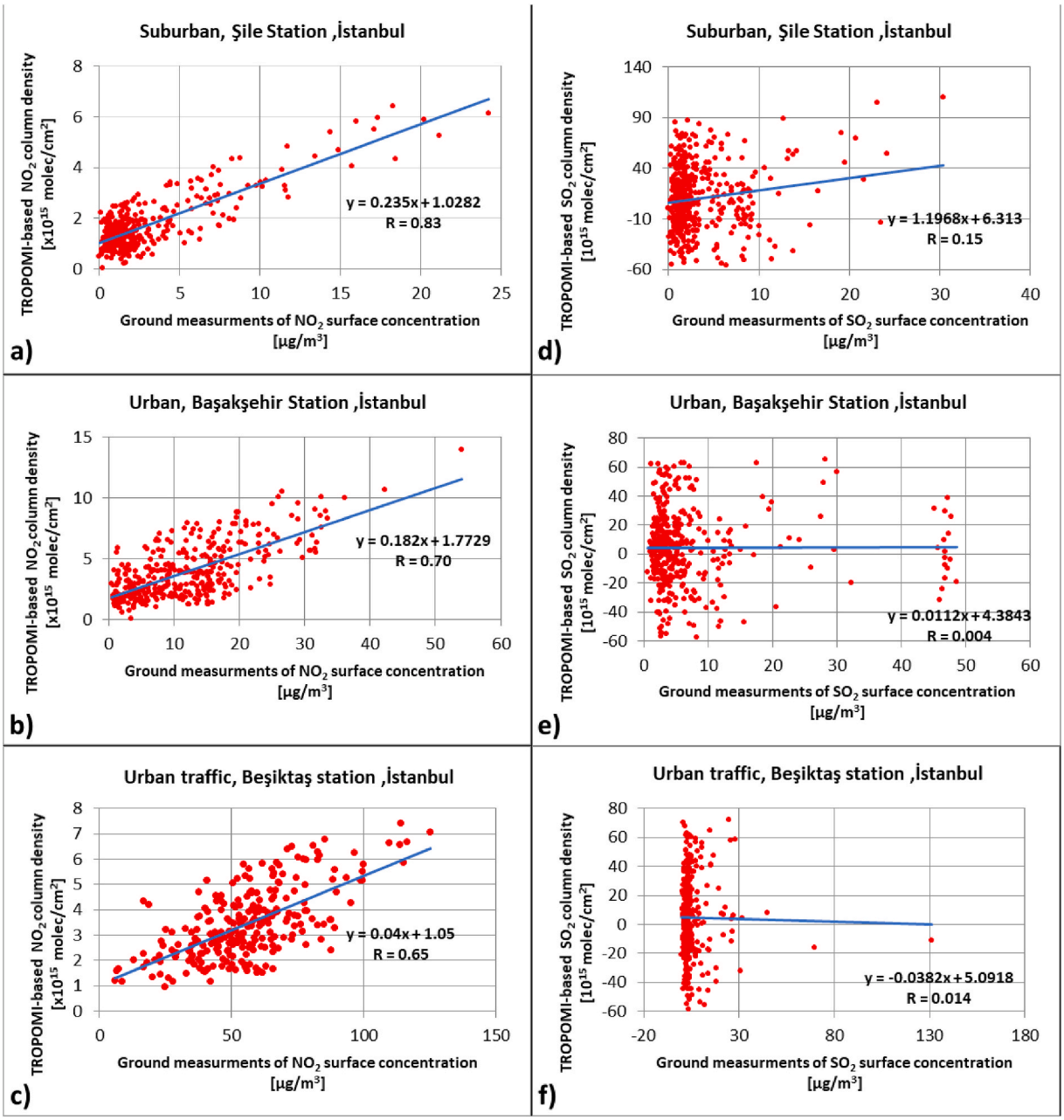

Fig. 10. Coherent of the hourly satellite-based tropospheric NO_2column number density derived from TROPOMI and the hourly ground-based measurements of NO_2 concentrations for tree sites as follows: suburban station, Şile, İstanbul (a); urban station, Başakşehir, İstanbul (b); urban traffic station, Beşiktaş, İstanbul (c).

zero correlation with AOD in 2019 and 2020, while moderate positive correlations with NO_2 and SO_2 in 2020. Considering the wind speed and air pollutant relations, low correlation coefficients were observed in 2019 for all variables; however, moderate negative correlation and high positive correlation was obtained from NO_2 (−0.56)- SO_2 (−0.65) and AOD (0.92), respectively, in 2020. Hence, these results are indicating the main contribution of meteorological parameters in decreasing air pollution. According to Ghahremanloo et al. (2020), while there was a relatively high correlation between daily NO_2 concentration and daily meteorological parameters, there was a relatively high correlation over four region of China in 2019, but the correlations have reduced in 2020 during the quarantine. However, these results indicate the lockdown period times were the major reasons for decreasing in NO_2 density.

4.7. Relationships between monthly average satellite-based air pollutants and PMI data

The PMI of a certain month is released on the first business day of the following month, and it mainly provides the earliest information about the economic performance, which is usually measured by Gross Domestic Product (GDP) (Tsuchiya, 2012). The PMI is also taken into account as a good indicator of industrial production, which is one of the most important indices for assessing economic conditions (Tsuchiya, 2012). Since industrial activities are sometimes shown as one of the main factors causing air pollution, we investigated if there is any correlation between PMI and satellite-derived pollutants. To the best of our knowledge, only one study investigated NO_2 pollution and PMI relationship during the February 2020 COVID-19 lockdown in China (Diamond and Wood, 2020). Diamond and Wood (2020) stated that the PMI and ln(NO_2) showed a pronounced and unprecedented decline in

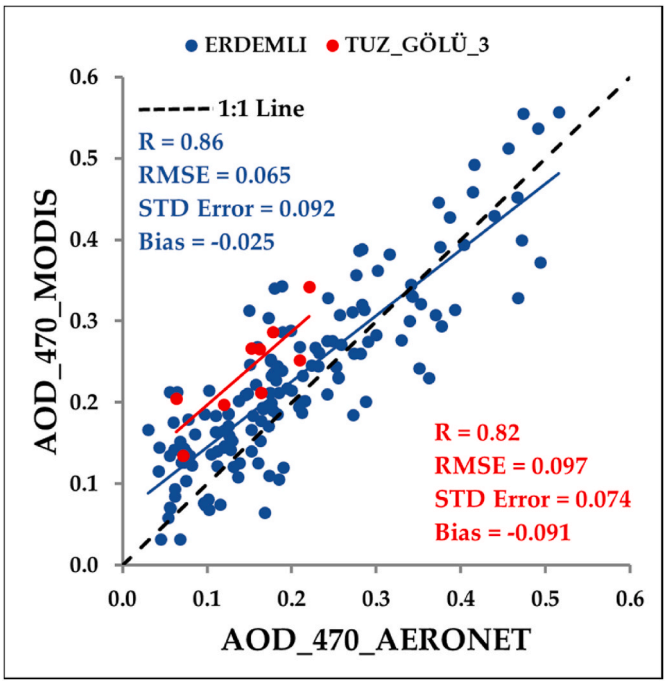

Fig. 11. Scatterplots between MODIS-derived AOD 470 nm and AERONET AOD 470 nm.

Table 5
Monthly average values for air temperature, surface pressure, total precipitation, wind speed, and air pollutants during the lockdown period over Turkey. The abbreviations Cor., Temp., Pres., Prec., and WS refer to correlation, air temperature (K), surface pressure (hPa), total precipitation (m) and wind speed (m/s), respectively.

Variables	2019			2020		
	Mar.	Apr.	May	Mar.	Apr.	May
NO_2	1.46	1.14	1.05	1.22	1.01	0.92
SO_2	13.83	5.38	4.44	15.93	9.39	4.90
AOD	0.10	0.19	0.18	0.12	0.13	0.18
Temp. (K)	278.77	282.40	289.92	280.43	283.22	288.72
Cor.(NO_2,Temp.)	−0.87			−0.92		
Cor.(SO_2,Temp.)	−0.81			−0.96		
Cor.(AOD,Temp.)	0.68			0.98		
Pres. (hPa)	890.35	890.42	890.77	890.34	890.31	891.74
Cor.(NO_2,Pres.)	−0.77			−0.73		
Cor.(SO_2,Pres.)	−0.70			−0.80		
Cor.(AOD,Pres.)	0.55			0.99		
Prec. (m)	0.07	0.09	0.05	0.09	0.07	0.08
Cor.(NO_2,Prec.)	0.29			0.55		
Cor.(SO_2,Prec.)	0.19			0.46		
Cor.(AOD,Prec.)	0.01			−0.01		
WS (m/s)	0.35	0.13	0.65	0.43	0.41	0.50
Cor.(NO_2,WS)	−0.28			−0.56		
Cor.(SO_2,WS)	−0.18			−0.65		
Cor.(AOD,WS)	−0.01			0.92		

February 2020 followed by a rapid recovery. In Turkey, almost more than 80% of economic activities are managed in Marmara and Aegean region. Therefore, in this analysis, the monthly PMI values were compared with the monthly average air pollutants of the Marmara and the Aegean regions. Fig. 12 presents the scatter plot (a) and bar charts (b-d) between monthly PMI and monthly average air pollutants. The time interval of this analysis covers from January 2019 to September 2020. It is clear from Fig. 12a that air pollutants and PMI does not have high correlation coefficients with NO_2 ($R = -0.08$), SO_2 ($R = -0.13$) and AOD ($R = 0.08$) proving that industrial activities do not have a high impact on air pollution on their own. Although Fig. 12b and c illustrate a decreasing trend in NO_2 and SO_2 associated with PMI values in the lockdown period, it is clear that this trend is similar in both 2019 and 2020, and the long-term variations in the PMI do not prove any relationship with air pollutants. Unlike NO_2 and SO_2 trend, AOD has an increasing trend related to the PMI in the lockdown period, but the same trend is also observed for the same period of the previous year. Besides, the long-term variations in the PMI again do not prove any relationship with AOD.

4.8. Discussion on the effect of COVID-19 on environmental sustainability and air quality

So far, many studies have emphasized the effect of the COVID-19 on the sustainable development of the environment (Shulla et al., 2021; Rume and Islam, 2020; Mukherjee et al., 2020; Praveena and Aris, 2021; Kumar et al., 2020). Rupani et al. (2020) published a detailed review about the COVID-19 and its natural environmental impacts, which is also illustrated in Fig. 13. In addition, Bherwani et al. (2021) analyzed the impact of the COVID-19 on Sustainable Development Goals (SDGs) of the United Nations in Indian subcontinent with a focus on air quality.

All these studies revealed that the measures taken to control the spread of the virus had both negative and positive effects on the environment globally (Fig. 14). Concerning the positive effects, there were noticeable improvements in air quality, and reduction in Greenhouse Gases (GHGs) emissions, water pollution and environmental noise. However, the pandemic had also negative sides such as the increase in medical waste and household plastics/waste, and careless and overusing of masks, gloves, and disinfectants.

These environmental effects of the COVID-19 are assumed not to last long time. Therefore, this pandemic provides an opportunity to develop a proper strategy for a better and long-term sustainable environmental management, and to determine sustainable solutions for further improvement in the air quality after the pandemic. Within this context, Fig. 15, for which detailed information is provided by Rume and Islam (2020), illustrates some possible strategies for global environmental sustainability.

5. Conclusion

In this study, the spatial-temporal patterns of Sentinel-5P TROPOMI-derived air pollutants, namely, NO_2 and SO_2, and MODIS-derived AOD are monitored and investigated between January 2019 and September 2020 including first wave lockdown period of COVID-19 outbreak over Turkey. The GEE platform is used for the retrieval and processing of satellite imagery, and data analysis.

According to the obtained results, NO_2 characteristically reach minimum values in the spring, then starting to increase in the summer and reaches maximum in the wintertime. Unlike NO_2, SO_2 becomes minimum in the whole spring and summer seasons. On the contrary, AOD is higher between the months of April and October than the others are. The NO_2 results from Sentinel-5P are highly correlated with the results from the ground stations. Besides, MODIS-derived AOD is very consistent with AERONET results. In addition, all the results have significant correlations with some meteorological parameters, especially pressure and temperature. Interestingly, the correlations with all parameters are higher in 2020.

The results and analyses show that temporal variations are more representative in NO_2 for the lockdown period of COVID19 outbreak. As seen from Figs. 3 and 4, NO_2 concentrations in the lockdown period of 2020 are significantly smaller than in the same period of 2019. After the lockdown, the concentrations leap higher levels than 2019, especially starting from July. The NO_2 concentrations are mainly affected by transportation, industrial and agricultural activities, heating in the wintertime, air conditioning need in the summertime. PMI analyses show that there are weak correlation between industrial activities and NO_2 concentration. The lockdown period covers the springtime in which

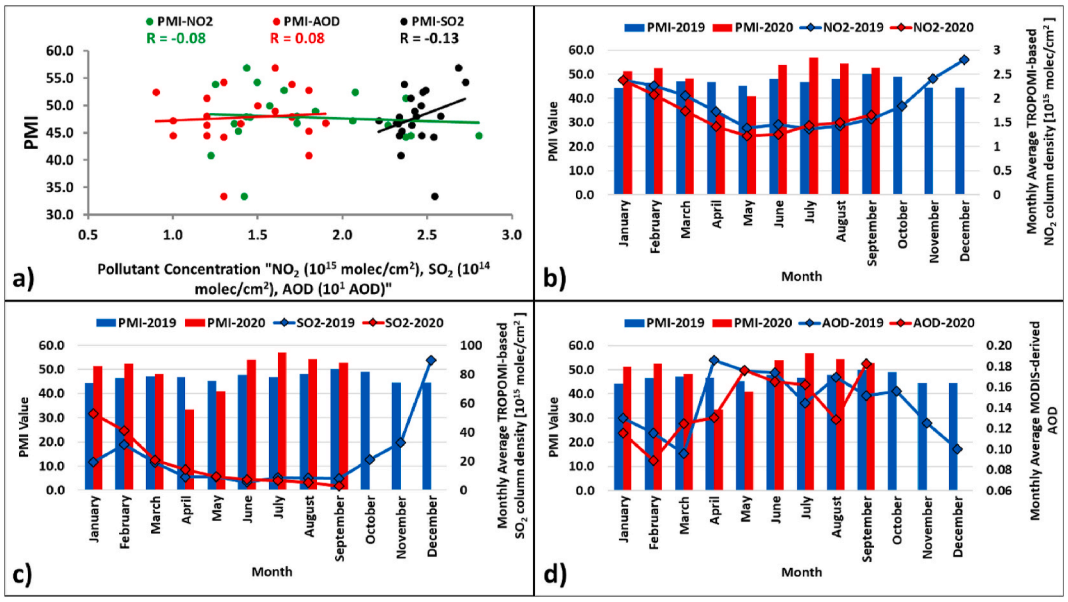

Fig. 12. The scatter plot (a) and bar charts (b–d) between monthly PMI and monthly average air pollutants.

Fig. 13. COVID-19 and its environmental impacts (Rupani et al., 2020).

heating, air conditioning agricultural needs are minimal. Therefore, it is considered that decreasing in transportation and industrial activities play the key role in decreasing NO_2 concentration during the lockdown period. The increase of the concentrations after the lock down coincides with the summer time. As seen from Fig. 3, spatial distribution of the NO_2 concentrations remarkably grows around the southern regions rather than the northern regions. They are the main touristic and agriculture regions in Turkey. In summer time, human population in touristic regions dramatically increases, so transportation and air-conditioning need also dramatically increase in these regions, especially in the southwestern part. For agriculture regions, irrigation, fertilization and stubble burning happen at the highest level in the summer time. As for the wintertime, it is understood the combustion increases due to house heating, which is the main parameter affecting the NO_2 concentration.

Unlike the decreasing trend of NO_2 in the lockdown period, the same significant decrease are not observed in SO_2 vertical column density and AOD during the whole lockdown period. Although, the AOD distribution significantly decreased only in April 2020, which the tightest restrictions were applied due to the COVID-19 outbreak, same period of 2019. These results reveal the lockdown had no effect on reducing effect on the vertical column density of SO_2. As in NO_2 analyses, the relationship between SO_2 and AOD, and meteorological/climatological parameters presents that air temperature and surface pressure have strong correlations with air pollutants, whereas precipitation and wind speed are not effective as well as air temperature and surface pressure. PMI correlation results also present almost no relationship with SO_2 and AOD showing economic/industrial activities do not have a high impact on the behavior of the air pollutants on their own. compared to the April 2019, the spatial distribution of SO_2 in the 2020 lockdown period had slightly higher concentrations.

This study is the first attempt to monitor and analyze the effects of the first wave COVID-19 lockdown period as well as on air pollution using satellite-derived air pollutants and their relationships with various parameters in Turkey at a national level. The analyses in this study show that air pollution variation due to human activity can be monitored most effectively through NO_2 concentration using satellite imageries. In this way, GEE provides a powerful and very effective platform for researchers to analyze these parameters. Processing Sentinel-5P data in this platform, it is found out that NO_2 concentration significantly decreased during the first wave lockdown period of COVID-19 outbreak. The further analyses of the results with other parameters, shows that the transportation and industrial activities played the key role in decreasing the NO_2 level. As for the summer time after the lockdown, agricultural and touristic activities caused to higher NO_2 levels. Thus, as a future work, the authors plan to investigate the relationship between air pollutants and with various parameters such as traffic density, touristic and agricultural statistics as well as with fatality cases of COVID-19 outbreak on the city level in Turkey.

CRediT authorship contribution statement

Fatemeh Ghasempour: Conceptualization, Methodology, Software, Validation, Formal analysis, Investigation, Writing – original draft, Writing – review & editing, Visualization. **Aliihsan Sekertekin:**

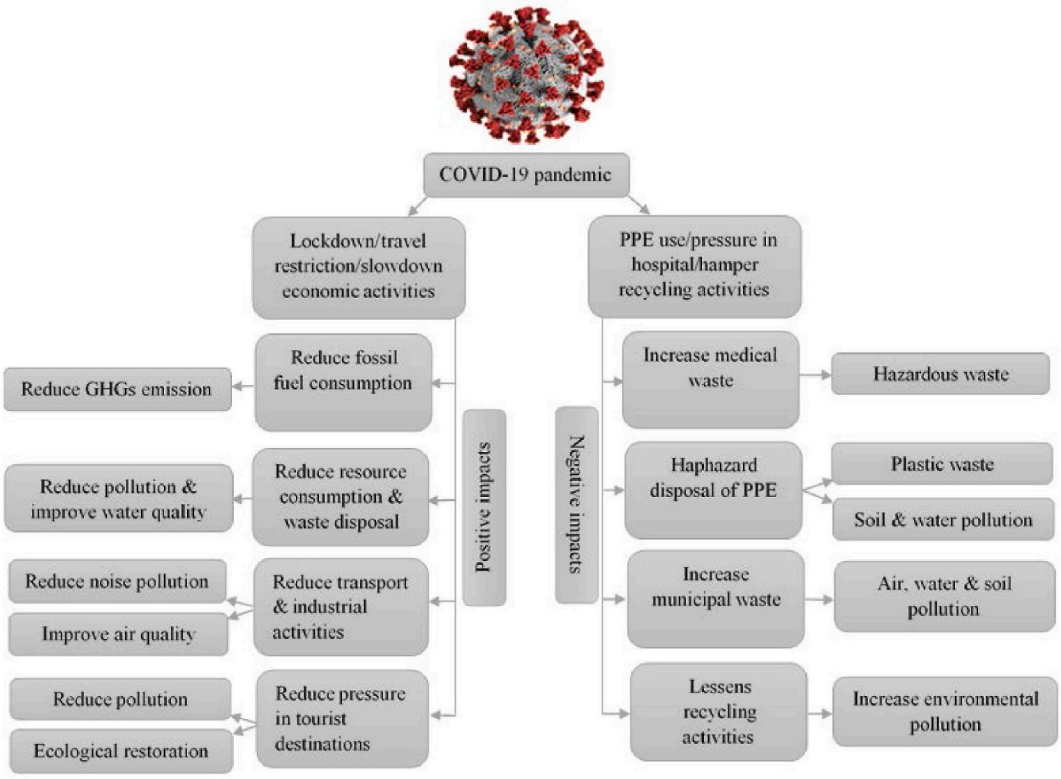

Fig. 14. Negative and positive environmental effects of COVID-19 pandemic (Rume and Islam, 2020).

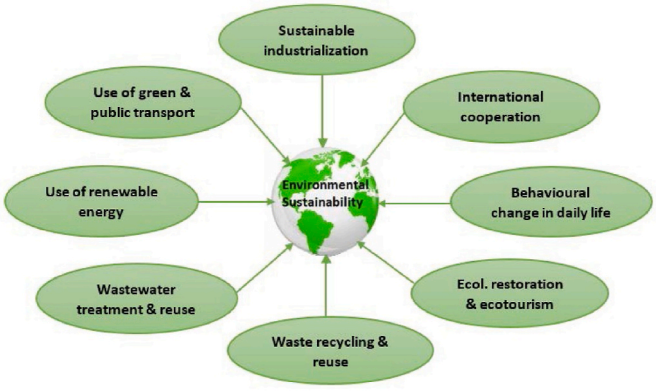

Fig. 15. Some possible strategies for global environmental sustainability (Rume and Islam, 2020).

Conceptualization, Supervision, Methodology, Formal analysis, Investigation, Writing – original draft, Writing – review & editing. **Senol Hakan Kutoglu:** Conceptualization, Writing – review & editing, Supervision.

Declaration of competing interest

The authors declare that they have no known competing financial interests or personal relationships that could have appeared to influence the work reported in this paper.

Acknowledgements

The authors would like to thank the GEE team and platform, and their collaborators (NASA, ESA, USGS, NOAA and so on) for providing the satellite imagery free of charge. The authors also thank NASA and Turkish Ministery of Environment and Urban Planning for enabling free access to AERONET and Air Quality Monitoring Center, respectively.

Appendix A. Supplementary data

Supplementary data to this article can be found online at https://doi.org/10.1016/j.jclepro.2021.128599.

References

Aksoy, S., Gorucu, O., Sertel, E., 2019. Drought monitoring using MODIS derived indices and Google Earth engine platform. In: 2019 8th International Conference on Agro-Geoinformatics (Agro-Geoinformatics). IEEE, pp. 1–6.

Aldabash, M., Bektas Balcik, F., Glantz, P., 2020. Validation of MODIS C6. 1 and MERRA-2 AOD using AERONET observations: a comparative study over Turkey. Atmosphere 11, 905.

Arya, S.P., 1999. Air Pollution Meteorology and Dispersion, vol. 6. Oxford University Press, New York.

Athanassiadou, M., Baker, J., Carruthers, D., Collins, W., Girnary, S., Hassell, D., et al., 2010. An assessment of the impact of climate change on air quality at two UK sites. Atmos. Environ. 44, 1877–1886.

Banerjee, T., Singh, S., Srivastava, R., 2011. Development and performance evaluation of statistical models correlating air pollutants and meteorological variables at Pantnagar, India. Atmos. Res. 99, 505–517.

Bherwani, H., Gautam, S., Gupta, A., 2021. Qualitative and quantitative analyses of impact of COVID-19 on sustainable development goals (SDGs) in Indian subcontinent with a focus on air quality. Int. J. Environ. Sci. Technol. 18 (4), 1019–1028.

Borsdorff, T., Hasekamp, O., Wassmann, A., Landgraf, J., 2014. Insights into Tikhonov regularization: application to trace gas column retrieval and the efficient calculation of total column averaging kernels. Atmospheric Measurement Techniques 7, 523.

Borsdorff, T., Hu, H., Hasekamp, O., Sussmann, R., Rettinger, M., Hase, F., et al., 2018. Mapping carbon monoxide pollution from space down to city scales with daily global coverage. Atmospheric Measurement Techniques 11, 5507–5518.

Borsdorff, T., Pandey, S., Hasekamp, O., Aben, I., Houweling, S., Landgraf, J., 2019. Carbon monoxide air pollution on sub-city scales and along arterial roads detected by the Tropospheric Monitoring Instrument. Atmos. Chem. Phys. 19.

Broomandi, P., Karaca, F., Nikfal, A., Jahanbakhshi, A., Tamjidi, M., Kim, J.R., 2020. Impact of COVID-19 event on the air quality in Iran. Aerosol and Air Quality Research 20, 1793–1804.

Bucsela, E., Perring, A., Cohen, R., Boersma, K., Celarier, E., Gleason, J., et al., 2008. Comparison of tropospheric NO2 from in situ aircraft measurements with near-real-time and standard product data from OMI. J. Geophys. Res.: Atmosphere 113.
Butz, A., Galli, A., Hasekamp, O., Landgraf, J., Tol, P., Aben, I., 2012. TROPOMI aboard Sentinel-5 Precursor: prospective performance of CH4 retrievals for aerosol and cirrus loaded atmospheres. Rem. Sens. Environ. 120, 267–276.
Cersosimo, A., Serio, C., Masiello, G., 2020. TROPOMI NO2 tropospheric column data: regridding to 1 km grid-resolution and assessment of their consistency with in situ surface observations. Rem. Sens. 12, 2212.
Chen, Zhongfei, Hao, Xinyue, Zhang, Xiaoyu, Chen, Fanglin, 2021. Have traffic restrictions improved air quality? A shock from COVID-19. J. Clean. Prod. 279, 123622 https://doi.org/10.1016/j.jclepro.2020.123622.
Clemente, J., Fontanelli, G., Ovando, G., Roa, Y., Lapini, A., Santi, E., 2020. Google Earth engine: application of algorithms for remote sensing of crops in tuscany (Italy). In: 2020 IEEE Latin American GRSS & ISPRS Remote Sensing Conference (LAGIRS). IEEE, pp. 195–200.
DeVries, B., Huang, C., Armston, J., Huang, W., Jones, J.W., Lang, M.W., 2020. Rapid and robust monitoring of flood events using Sentinel-1 and Landsat data on the Google Earth Engine. Rem. Sens. Environ. 240, 111664.
Diamond, M.S., Wood, R., 2020. Limited regional aerosol and cloud microphysical changes despite unprecedented decline in nitrogen oxide pollution during the February 2020 COVID-19 shutdown in China. Geophys. Res. Lett. 47 e2020GL088913.
Eckhoff, R.K., 2009. Understanding dust explosions. The role of powder science and technology. J. Loss Prev. Process. Ind. 22, 105–116.
El Khoury, E., Ibrahim, E., Ghanimeh, S., 2019. A look at the relationship between tropospheric nitrogen dioxide and aerosol optical thickness over Lebanon using spaceborne data of the Copernicus programme. In: 2019 Fourth International Conference on Advances in Computational Tools for Engineering Applications (ACTEA). IEEE, pp. 1–6.
Elshorbany, Y.F., Kapper, H.C., Ziemke, J.R., Parr, S.A., 2021. The status of air quality in the United States during the COVID-19 pandemic: a remote sensing perspective. Rem. Sens. 13, 369.
Eren, O., 2014. Forecasting the relative direction of economic growth by using the purchasing ManagersIndex. Iktisat Isletme ve Finans 29, 55–72.
Fan, C., Li, Y., Guang, J., Li, Z., Elnashar, A., Allam, M., et al., 2020. The impact of the control measures during the COVID-19 outbreak on air pollution in China. Rem. Sens. 12, 1613.
Feng, Y., Chen, D., Zhang, X., 2019. Atmospheric aerosol pollution across China: a spatiotemporal analysis of satellite-based aerosol optical depth during 2000–2016. International Journal of Digital Earth 12, 843–857.
Filonchyk, M., Yan, H., 2019. Urban Air Pollution Monitoring by Ground-Based Stations and Satellite Data,©. Springer.
Fioletov, V., McLinden, C.A., Griffin, D., Theys, N., Loyola, D.G., Hedelt, P., et al., 2020. Anthropogenic and Volcanic Point Source SO_2 Emissions Derived from TROPOMI on Board Sentinel-5 Precursor: First Results.
Ghahremanloo, M., Lops, Y., Choi, Y., Mousavinezhad, S., 2020. Impact of the COVID-19 outbreak on air pollution levels in East Asia. Sci. Total Environ. 142226.
Ghasempour, Fatemeh, Sekertekin, Aliihsan, Kutoglu, Hakan, 2021. Effect of first wave COVID-19 outbreak lockdown measures on satellite-based tropospheric NO2 over Mersin Province, Turkey. Intercontinental Geoinformation Days (IGD) 16–19.
Giles, D.M., Sinyuk, A., Sorokin, M.G., Schafer, J.S., Smirnov, A., Slutsker, I., et al., 2019. Advancements in the Aerosol Robotic Network (AERONET) Version 3 database–automated near-real-time quality control algorithm with improved cloud screening for Sun photometer aerosol optical depth (AOD) measurements. Atmospheric Measurement Techniques 12.
Grey, W.M., North, P.R., Los, S.O., Mitchell, R.M., 2006. Aerosol optical depth and land surface reflectance from multiangle AATSR measurements: global validation and intersensor comparisons. IEEE Trans. Geosci. Rem. Sens. 44, 2184–2197.
Gupta, P., Levy, R.C., Mattoo, S., Remer, L.A., Munchak, L.A., 2016. A surface reflectance scheme for retrieving aerosol optical depth over urban surfaces in MODIS Dark Target retrieval algorithm. Atmospheric Measurement Techniques 9, 3293–3308.
Hajiloo, F., Hamzeh, S., Gheysari, M., 2019. Impact assessment of meteorological and environmental parameters on PM 2.5 concentrations using remote sensing data and GWR analysis (case study of Tehran). Environ. Sci. Pollut. Control Ser. 26, 24331–24345.
He, W., Wang, Y., Zuo, J., Luo, Y., 2017. Sectoral linkage analysis of three main air pollutants in China's industry: comparing 2010 with 2002. J. Environ. Manag. 202, 232–241.
Huang, H., Chen, Y., Clinton, N., Wang, J., Wang, X., Liu, C., et al., 2017. Mapping major land cover dynamics in Beijing using all Landsat images in Google Earth Engine. Rem. Sens. Environ. 202, 166–176.
Huijnen, V., Eskes, H., Amstrup, B., Bergstrom, R., Boersma, K., Elbern, H., et al., 2009. Comparison of OMI NO2 tropospheric columns with an ensemble of global and European regional air quality models. Atmos. Chem. Phys. Discuss. 9, 22271–22330.
Ialongo, I., Virta, H., Eskes, H., Hovila, J., Douros, J., 2020. Comparison of TROPOMI/Sentinel-5 Precursor NO2 observations with ground-based measurements in Helsinki. Atmospheric Measurement Techniques 13.
Ji, M., Jiang, Y., Han, X., Liu, L., Xu, X., Qiao, Z., et al., 2020. Spatiotemporal relationships between air quality and multiple meteorological parameters in 221 Chinese cities. Complexity 2020.
Kanniah, K.D., Zaman, N.A.F.K., Kaskaoutis, D.G., Latif, M.T., 2020. COVID-19's impact on the atmospheric environment in the Southeast Asia region. Sci. Total Environ. 139658.
Kaplan, Gordana, Yigit Avdan, Zehra, 2020. Space-Borne air pollution observation from sentinel-5p tropomi: relationship between pollutants, geographical and demographic data. Int. J. Eng. Geosci. 5 (3), 130–137. https://doi.org/10.26833/ijeg.644089.
Karuppasamy, M.B., Seshachalam, S., Natesan, U., Ayyamperumal, R., Karuppannan, S., Gopalakrishnan, G., et al., 2020. Air pollution improvement and mortality rate during COVID-19 pandemic in India: global intersectional study. Air Quality, Atmosphere & Health 13, 1375–1384.
Kramer, L.J., Leigh, R.J., Remedios, J.J., Monks, P.S., 2008. Comparison of OMI and ground-based in situ and MAX-DOAS measurements of tropospheric nitrogen dioxide in an urban area. J. Geophys. Res.: Atmosphere 113.
Kumar, A., Malla, M.A., Dubey, A., 2020. With Corona outbreak: nature started hitting the reset button globally. Frontiers in public health 8, 569353.
Laat, Ad, Vazquez-Navarro, M., Theys, N., Stammes, P., 2020. Analysis of properties of the 19 February 2018 volcanic eruption of Mount Sinabung in S5P/TROPOMI and Himawari-8 satellite data. Nat. Hazards Earth Syst. Sci. 20, 1203–1217.
Landgraf, J., aan de Brugh, J., Borsdorff, T., Houweling, S., Hasekamp, O., 2018. Algorithm Theoretical Baseline Document for Sentinel-5 Precursor: Carbon Monoxide Total Column Retrieval. ESA.
Leinonen, U., Koskinen, J., Makandi, H., Mauya, E., Käyhkö, N., 2018. Open foris and google earth engine linking expert PARTICIPATIONWITH natural resource mapping and remote sensing training IN Tanzania. International Archives of the photogrammetry. Remote Sensing & Spatial Information Sciences 42.
Lin, C.-A., Chen, Y.-C., Liu, C.-Y., Chen, W.-T., Seinfeld, J.H., Chou, C.C.-K., 2019. Satellite-derived correlation of SO2, NO2, and aerosol optical depth with meteorological conditions over East Asia from 2005 to 2015. Rem. Sens. 11, 1738.
Lorente, A., Boersma, K., Eskes, H., Veefkind, J., Van Geffen, J., de Zeeuw, M., et al., 2019. Quantification of nitrogen oxides emissions from build-up of pollution over Paris with TROPOMI. Sci. Rep. 9, 1–10.
Lorente, A., Boersma, K.F., Yu, H., Dörner, S., Hilboll, A., Richter, A., et al., 2017. Structural uncertainty in air mass factor calculation for NO2 and HCHO satellite retrievals. Atmospheric Measurement Techniques 10, 759–782.
Mesas-Carrascosa, F.-J., Pérez Porras, F., Triviño-Tarradas, P., García-Ferrer, A., Meroño-Larriva, J.E., 2020. Effect of lockdown measures on atmospheric nitrogen dioxide during SARS-CoV-2 in Spain. Rem. Sens. 12, 2210.
Metya, A., Dagupta, P., Halder, S., Chakraborty, S., Tiwari, Y.K., 2020. COVID-19 lockdowns improve air quality in the south-east Asian regions, as seen by the remote sensing satellites. Aerosol and Air Quality Research 20.
Mukherjee, A., Babu, S.S., Ghosh, S., 2020. Thinking about water and air to attain sustainable development goals during times of COVID-19 pandemic. Journal of Earth System Science 129, 1–8.
Nakada, L.Y.K., Urban, R.C., 2020. COVID-19 pandemic: impacts on the air quality during the partial lockdown in São Paulo state, Brazil. Sci. Total Environ. 730, 139087.
Nichol, J.E., Bilal, M., Ali, M., Qiu, Z., 2020. Air pollution scenario over China during COVID-19. Rem. Sens. 12, 2100.
O'Brien, D.M., Polonsky, I.N., Utembe, S., Rayner, P., 2016. Remote Sensing CO2, CH4 and CO Emissions in a Polluted Urban Environment.
Ogen, Y., 2020. Assessing nitrogen dioxide (NO2) levels as a contributing factor to the coronavirus (COVID-19) fatality rate. Sci. Total Environ. 138605.
Omrani, H., Omrani, B., Parmentier, B., Helbich, M., 2020. Spatio-temporal data on the air pollutant nitrogen dioxide derived from Sentinel satellite for France. Data in brief 28, 105089.
Othman, Murnira, Latif, Mohd Talib, 2021. Air pollution impacts from COVID-19 pandemic control strategies in Malaysia. J. Clean. Prod. 291, 125992 https://doi.org/10.1016/j.jclepro.2021.125992.
Otmani, A., Benchrif, A., Tahri, M., Bounakhla, M., El Bouch, M., Mh, Krombi, 2020. Impact of covid-19 lockdown on PM10, SO2 and NO2 concentrations in salé city (Morocco). Sci. Total Environ. 735, 139541.
Perera, F.P., 2017. Multiple threats to child health from fossil fuel combustion: impacts of air pollution and climate change. Environ. Health Perspect. 125, 141–148.
Pinardi, G., Vigouroux, C., Langerock, B., De Mazière, M., Granville, J., Lambert, J.-C., et al., 2018. Sentinel-5 Precursor NO2 and HCHO validation using NDACC and complementary UV-Vis DOAS systems. Geophysical Research Abstracts 20, EGU2018-15991.
Praveena, S.M., Aris, A.Z., 2021. The impacts of COVID-19 on the environmental sustainability: a perspective from the Southeast Asian region. Environ. Sci. Pollut. Control Ser. 1–8.
Qiao, Z., Wu, F., Xu, X., Yang, J., Liu, L., 2019. Mechanism of spatiotemporal air quality response to meteorological parameters: a national-scale analysis in China. Sustainability 11, 3957.
Rojas, J.P., Urdanivia, F.R., Garay, R.A., García, A.J., Enciso, C., Medina, E.A., et al., 2021. Effects of COVID-19 pandemic control measures on air pollution in Lima metropolitan area, Peru in South America. Air Quality, Atmosphere & Health 1–9.
Rume, T., Islam, S.D.U., 2020. Environmental effects of COVID-19 pandemic and potential strategies of sustainability. Heliyon 6, e04965.
Ruoying, C., Jun, Z., Wen, L., Jingjing, J., 2019. Temporal and spatial distribution of SO2 in the process of haze in north China based on remote sensing data. Int. J. Environ. Monit. Anal. 7, 27.
Rupani, P.F., Nilashi, M., Abumalloh, R.A., Asadi, S., Samad, S., Wang, S., 2020. Coronavirus pandemic (COVID-19) and its natural environmental impacts. Int. J. Environ. Sci. Technol. 1–12.
Salmabadi, H., Saeedi, M., 2019. Monitoring of SO2 column concentration over Iran using satellite-based observations during 2005-2016. Pollution 5, 257–268.
Shulla, K., Voigt, B.F., Cibian, S., Scandone, G., Martinez, E., Nelkovski, F., Salehi, P., 2021. Effects of COVID-19 on the sustainable development goals (SDGs). Discover Sustainability 2, 15.

Smirnov, A., Holben, B., Eck, T., Dubovik, O., Slutsker, I., 2000. Cloud-screening and quality control algorithms for the AERONET database. Rem. Sens. Environ. 73, 337–349.

Tobías, A., Carnerero, C., Reche, C., Massagué, J., Via, M., Minguillón, M.C., et al., 2020. Changes in air quality during the lockdown in Barcelona (Spain) one month into the SARS-CoV-2 epidemic. Sci. Total Environ. 138540.

Tsuchiya, Y., 2012. Is the purchasing managers' index useful for assessing the economy's strength? A directional analysis. Econ. Bull. 32.

Tzortziou, M., Parker, O., Lamb, B., Herman, J.R., Lamsal, L., Stauffer, R., et al., 2018. Atmospheric Trace Gas (NO2 and O3) variability in South Korean coastal waters, and implications for remote sensing of coastal ocean color dynamics. Rem. Sens. 10, 1587.

Van Geffen, J., Eskes, H., Boersma, K., Maasakkers, J., Veefkind, J., 2018. TROPOMI ATBD of the Total and Tropospheric NO2 Data Products (Issue 1.2. 0). Royal Netherlands Meteorological Institute (KNMI), De Bilt, the Netherlands s5P-KNMI-L2-0005-RP.

Veefkind, J., Aben, I., McMullan, K., Förster, H., De Vries, J., Otter, G., et al., 2012. TROPOMI on the ESA Sentinel-5 Precursor: a GMES mission for global observations of the atmospheric composition for climate, air quality and ozone layer applications. Rem. Sens. Environ. 120, 70–83.

Vîrghileanu, M., Săvulescu, I., Mihai, B.-A., Nistor, C., Dobre, R., 2020. Nitrogen dioxide (NO2) pollution monitoring with sentinel-5P satellite imagery over Europe during the coronavirus pandemic outbreak. Rem. Sens. 12, 3575.

Wang, G., Deng, X.-J., Wang, C.-L., Zhang, X.-Y., Yan, H.-H., Chen, D.-H., et al., 2019. A new and detailed assessment of the spatiotemporal characteristics of the SO2 distribution in the pearl river delta region of China and the effect of SO2 emission reduction. Aerosol and Air Quality Research 19, 1900–1910.

Wei, J., Li, Z., Peng, Y., Sun, L., 2019. MODIS Collection 6.1 aerosol optical depth products over land and ocean: validation and comparison. Atmos. Environ. 201, 428–440.

Wu, X., Zhang, X., Chuai, X., Huang, X., Wang, Z., 2019. Long-term trends of atmospheric CH4 concentration across China from 2002 to 2016. Rem. Sens. 11, 538.

Xia, H., Zhao, J., Qin, Y., Yang, J., Cui, Y., Song, H., et al., 2019. Changes in water surface area during 1989–2017 in the huai river basin using Landsat data and Google Earth engine. Rem. Sens. 11, 1824.

Xu, J., Heue, K., Coldewey-Egbers, M., Romahn, F., Doicu, A., Loyola, D., 2018. Full-Physics Inverse Learning Machine for satellite remote sensing of ozone profile shapes and tropospheric columns. Int. Arch. Photogram. Rem. Sens. Spatial Inf. Sci. 42, 3.

Xu, R., Lin, B., 2017. Why are there large regional differences in CO2 emissions? Evidence from China's manufacturing industry. J. Clean. Prod. 140, 1330–1343.

Zhang, G., Xu, H., Wang, H., Xue, L., He, J., Xu, W., et al., 2020a. Exploring the inconsistent variations in atmospheric primary and secondary pollutants during the G20 2016 Summit in Hangzhou, China: 2 implications from observation and model 3. Atmos. Chem. Phys. https://doi.org/10.5194/acp-2019-1061, 1e25.

Zhang, T., Cao, H., Song, H., Shi, H., 2020b. Validation of MODIS C6 aerosol optical depth in China. In: IOP Conference Series: Materials Science and Engineering, vol. 780. IOP Publishing, p. 42045.

Zhang, Z., Arshad, A., Zhang, C., Hussain, S., Li, W., 2020c. Unprecedented temporary reduction in global air pollution associated with COVID-19 forced confinement: a continental and city scale analysis. Rem. Sens. 12, 2420.

Zheng, Z., Yang, Z., Wu, Z., Marinello, F., 2019. Spatial variation of NO2 and its impact factors in China: an application of sentinel-5P products. Rem. Sens. 11, 1939.